Evaluating the Performance of a Solar Thermal Field: A Case Study with Proposed Improvements

Author:
Anton Segovia Lundh, an2108lu-s@student.lu.se

Supervisors:
LTH: Jens Klingmann
RISE: Patrik Ollas and Zack Norwood
Absolicon: Joakim Byström and Benjamin Ahlgren

Examiner:
LTH: Martin Andersson

Department of Energy Sciences, Faculty of Engineering LTH,
Lund University, SE-221 00 Lund, Sweden

Abstract

Given the urgency of climate change, alternative energy sources, and policy strategies are needed to reach the net-zero emission goals and halt global warming. Solar thermal energy is a renewable and abundant energy source that could be a part of the solution. In this master's thesis, the performance of a pilot solar thermal park in northern Sweden was modeled and evaluated based on an international evaluation standard, ISO 24194:2022 'Solar energy — Collector fields — Check of performance'. However, due to simplifications and uncertainties in the ISO 24194:2022, a broader analysis of both the solar thermal field and the ISO 24194:2022 was made. A fault in the ISO 24194:2022 was found which makes the measured performance appear better if worse sensor maintenance and equipment were used. A suggestion for this problem was changing a parameter in the ISO 24914:2022 to mark certainty/consistency in the performance evaluation rather than impacting the actual performance calculation. By applying the ISO 24194:2022 and color coding the performance data of the solar thermal park by hour it was shown that the performance of the park had a significant dip in the middle of the day. A possible reason for this could be non-ideal tracking which is most noticeable in the middle of the day. If the tracking system would be fixed a performance increase of 2-3 % is plausible. It was also found that the park had unnecessary heat losses from the pipes above ground, which if insulated correctly could improve performance by a further 3%. Adding these improvements together a total increase in performance of 4-5% is expected, which relates to 15-20 kW.

Acknowledgments

I am grateful for the time and energy provided by all of my supervisors at LTH, RISE, and Absolicon.

A special thanks to Patrik Ollas and Zack Norwood for providing your expertise in solar thermal and performance models. You brought a lot of good questions, encouragement, and knowledge into this master's thesis.

I would also like to acknowledge the energy and motivation Joakim Byström brought in when joining the project halfway in. I also wish to thank you for helping with specific questions regarding the solar thermal field.

Finally, I would like to thank my aunt, Magdalena Lundh Boork, for providing her meticulous feedback, and encouragement for the writing of this master's thesis.

It has been my pleasure to work with all of you.

Contents

Nomenclature

Performance calculations

$\dot{Q}_{estimate}$	Estimated power production	[W]
$\eta_{0,b}$	Collector peak efficiency	[−]
$a_{1,\Delta Q}$	Heat loss coefficient	[W/(m^{2}K)]
a_5	Effective thermal capacity	[J/(m^{2}K)]
A_{GF}	Gross area of collector field	[m^2]
G_b	Beam irradiance (direct irradiance)	[W/m^2]
G_d	Diffuse irradiance	[W/m^2]
$K_b(\theta_L, \theta_T)$	Incidence angle modifier for direct solar irradiance	[−]
K_d	Incidence angle modifier for diffuse solar radiation	[−]
q_{1-pipe}	Empirical specific heat losses per m pipe	[°C]
T_a	Ambient air temperature	[°C]
T_m	Mean temperature of heat transfer fluid in collector loop	[°C]
$T_{\Delta Q}$	Temperature dependence of the heat loss coefficient	[°C]

Heat loss calculations

λ_g	Thermal conductivity of ground	[W/(m°C)]
λ_i	Thermal conductivity of insulation	[W/(m°C)]
λ_p	Thermal conductivity of pipe	[W/(m°C)]
h	Convective heat transfer coefficient of air	[W/(m^2°C)]

L_{pipe}	Total length of pipe system without collectors	[m]
Q_{total}	Total heat losses	[W]
R_c	Temperature field	[m^2°C/W]
R_f	Convection resistance of pipe in two dimensions	[m°C/W]
R_g	The ground resistance	[m^2°C/W]
R_i	Conduction resistance of insulation in two dimensions	[m°C/W]
r_i	Inner radius of pipe	[m]
r_o	Outer radius of pipe	[m]
R_p	Conduction resistance of pipe in two dimensions	[m°C/W]
R_{total}	Total resistance of pipe system in two dimensions	[m°C/W]
T_a	Ambient air temperature	[°C]
T_m	Mean temperature of heat transfer fluid in collector loop	[°C]
T_r	Return temperature of heat transfer fluid from heat exchanger	[°C]
T_s	Supply temperature of heat transfer fluid to heat exchanger	[°C]

1 Introduction

We humans are the main driver of climate change due to the heavy use of CO_2 intensive energy sources such as coal and oil [1]. Achieving net-zero emissions and halting global warming requires a change in how we use and generate energy. Among the alternatives is solar energy which is an abundant energy source that humans have utilized throughout history. Traditionally, the solar role in society has mainly been heating our planet, growing our crops, and in a religious context, symbolizing life [2]. As human technology evolved experiments on harnessing the sun's energy have emerged, where concentrating solar collectors (CSP) are becoming more common in solar thermal systems [3].

Globally, heat accounts for fifty percent of the final energy consumption with 10% percent being renewables [3]. Even so, the solar thermal market has been declining for the last decade, until 2021 when the installed capacity increased by 3% [4]. This increase could continue, motivated by governments who are strengthening policies to reduce reliance on fossil fuels for heating due to concerns in energy affordability, geopolitics, and emission reduction [5]. International collaboration on heating has also been accelerated due to the ongoing energy crisis, which was further aggravated by Russia's invasion of Ukraine [5]. As of now, financial policies are the most common type of policy to encourage renewable heating globally. However, the International Energy Agency (IEA) [5] recommends policymakers to also establish long-term heating strategies that align with the net-zero emission scenario.

Introducing new standards, regulations, and testing procedures that long-term consistency for performance testing could increase the market for solar thermal in the long-term by building consumer trust [6]. It is important that the performance testing is done under similar conditions, using the same parameters, and appropriate instruments, to make the performance comparison fair between products [6]. In 2022 the International Organization for Standardization (ISO) therefore released their first standard used for performance evaluation for a whole solar thermal collector field, ISO 24194:2022 [7], titled 'Solar energy — Collector fields — Check of performance'.

The ISO 24194:2022 will be studied in this master's thesis to evaluate the performance of a solar thermal collector field in the middle of Sweden. The solar thermal park is called *Högslätten 2023 Solar Thermal Park* and is built as a pilot project by the Swedish solar thermal company Absolicon in partnership with the Swedish Energy Agency (Energimyndigheten) to showcase the potential of large-scale solar thermal in Sweden. The evaluation will be based on the ISO 24194:2022 together with expertise from Research Institutes of Sweden (RISE) and Absolicon.

1.1 Previous studies on performance calculations

This section highlights and gives a summary of two relevant previous studies, no extensive literature review is presented.

An earlier performance model at Absolicon was developed by a student, E. Magnusson [8], doing her master's thesis with Absolicon and RISE in 2022. It was based on the previous standard for evaluation of solar thermal, ISO 9806:2017, which provides methods for testing individual collectors, thus not a whole collector field. RISE then further improved and developed E. Magnusson models and further looked into using the newly released ISO 24194:2022 [9].

In 2019 a study by V. Unterberger, et al. [10] on adaptive short-term forecasting on energy yield for a solar collector field was done. They found that the current research in forecasting energy yield for solar thermal was inadequate and wanted a standard for evaluating a solar thermal park with the following requirements: simple implementation, automatic adaption to seasonal changes, and wide applicability. They, therefore, made a model themselves where they could predict the solar thermal performance within an absolute range normalized error of about 5% with the use of real weather data. They claim that their results were nearly twice as accurate as the current common forecasting methods at that time.

1.2 Contribution

The purpose of this master's thesis is to improve an existing model for evaluating the performance of *Högslätten 2023 Solar Thermal Park* with the use of the new international standard for validation of performance for solar thermal parks, the ISO 24194:2022. The areas that mainly will be investigated for the new evaluation model are heat losses in pipes and the impact of shadows on the solar collectors. With the results from the performance evaluation suggestions on improving the performance will also be given.

As more and more knowledge and time went into the research of this master's thesis more and more questions about the feasibility of verifying a solar collector park with the ISO 24194:2022 emerged; why have certain simplifications been made and how do these simplifications change the verification of the solar collector field? How is the geographic location of the solar park impacting the results of the ISO? These questions could be boiled down to "How feasible is it to use an international standard for evaluating a solar thermal park with concentrated solar panels in a cold climate, with relatively low direct sunlight, and few hours of sun in the winter?". Therefore, a sensitivity analysis together with the main performance calculations will be made in this master's thesis.

2 Evaluated project

The evaluated solar thermal park is called *Högslätten 2023 Solar Thermal Park* and is built at Högslätten, Härnösand, northern Sweden by the Swedish solar thermal company Absolicon. The park is planned to be finished in 2023 and is estimated to produce 1 000 MWh of heat each year for a district heating system in Härnösand. To financially support the project the Swedish Energy Agency has provided €800 000 towards the solar thermal park, and RISE is assisting with research and knowledge. When finished, the park will act as a pilot and demonstration program for large-scale solar thermal in Sweden.

As of January 2023 the construction of the project is not completely finished and is divided into two building phases, see Figure 1. Phase 1 is the subject of evaluation for this master's thesis and was put into operation in September 2022 with a collector area of 1056 m^2, an estimated capacity of 0.5 MW, and is expected to deliver 330 MWh of heat each year to the district heating system in Härnösand. A technical house for the integration of district heating, data collection, and hosting visits was also built in Phase 1. Phase 2 is expected to be done in 2023 with a capacity of 1 MW, expected delivery of 660 MWh heat, and a collector area of around 2000 m^2 [11]. Phase 1 and Phase 2 are pictured in Figure 1 with collector area and power output.

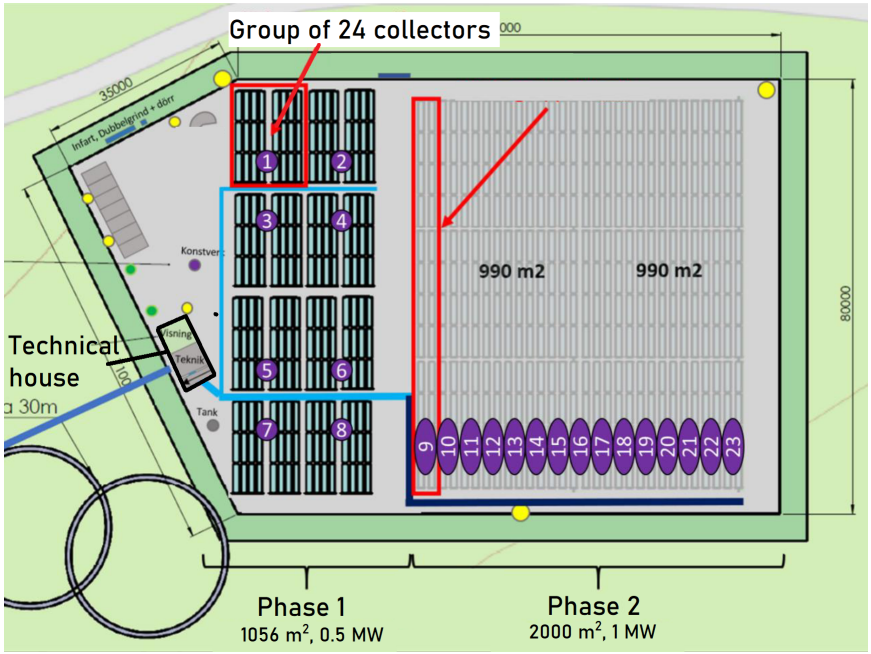

Figure 1: Picture representing Phase 1 and Phase 2. To the very left is the technical house. Next to the technical house is Phase 1: collector area of 1056 m^2. To the right are the plans for Phase 2: an additional 2000 m^2 collector area.

2.1 Solar thermal collectors, *Absolicon T160*

The solar collectors used at Högslätten 2023 Solar Thermal Park are the Absolicon T160's, see Figure 2. The Absolicon T160's is Absolicon's developed parabolic trough collector (PTC) which can deliver heat, steam, and cooling up to 160 °C for industries and district heating [12]. The main collector parts are: concentrator, tracking system, and absorber. The concentrator directs the solar radiation onto the absorber which transfers the thermal energy to a fluid inside the absorber. When the fluid gets heated it is directed through a pipe system to a heat exchanger that delivers the energy to the district heating system [12]. The tracking system is a one-axis solar tracking system, made by Siemens, that follows the path of the sun and maximizes the amount of direct sunlight onto the collector [12]. The collectors are also modular which makes it possible to start Phase 1 while still building Phase 2. A picture of the solar collectors used at Högslätten, displayed with absorber, tracking system, and concentrator can be seen in Figure 2.

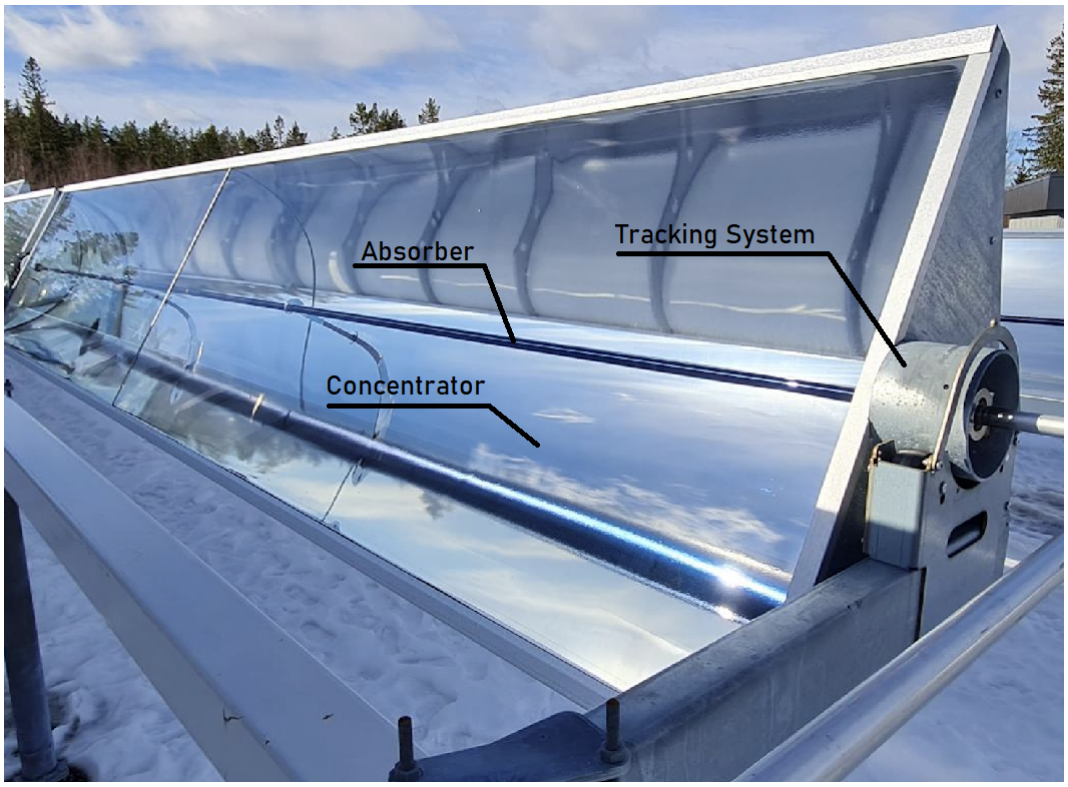

Figure 2: Picture of an installed Absolicon T160 at Högslätten Solar Thermal Park [13], displayed with absorber, tracking system, and concentrator.

The Absolicon T160 is certified by Solar Keymark. Solar Keymark has developed a standard for testing and certifying the performance of singular collectors in a lab environment [14]. The Solar Keymark test results on the Absolicon T160 can be seen in Table 1.

Table 1: Absolicon T160 test results from Solar Keymark [14] where performance parameters and dimensions are measured. Figure taken from Solar Keymark [14]

Collector Type					Concentrating collector					
Collector name	Gross area (A_G)	Gross length	Gross width	Gross height	Power output per collector Gb = 850 W/m2, Gd = 150 W/m2 & u = 1.3 m/s $\vartheta_m - \vartheta_a$					
					0 K	10 K	30 K	50 K	70 K	180 K
	m²	mm	mm	mm	W	W	W	W	W	W
T160	6.04	1'095	5'514	5.51	3'654	3'610	3'522	3'434	3'346	2'861
Power output per m² gross area					605	598	583	568	554	474

Performance parameters test method	Quasi dynamic									
Performance parameters (related to A_G)	η0, b	a1	a2	a3	a4	a5	a6	a7	a8	Kd
Units	-	W/(m²K)	W/(m²K²)	J/(m³K)	-	J/(m²K)	s/m	W/(m²K⁴)	W/(m²K⁴)	-
Test results	0.697	0.73	0.000	0.000	0.00	1'483	0.000	0.00	0.0E+00	0.12
Incidence angle modifier test method		Quasi dynamic - outdoor								
Incidence angle modifier	Angle	10°	20°	30°	40°	50°	60°	70°	80°	90°
Transversal	$K_{\theta T,coll}$	1.00	1.00	1.00	1.00	1.00	1.00	1.00	1.00	0.00
Longitudinal	$K_{\theta L,coll}$	0.99	0.99	0.98	0.96	0.91	0.77	0.53	0.18	0.00

2.2 Pipe system

To transport the heat in the pipe system a fluid is used, in this solar thermal park a mix of 35% propylene glycol and 65% water. The fluid is in a closed loop where it goes into every collector group, gets heated, and passes through the collector pipes. It continues through underground pipes to the technical house where a heat exchanger transfers the heat from the fluid to the district heating system, and then back to the collectors again. The piping system consists of pipes between the collectors, between the collector groups, and underground pipes.

2.2.1 Pipes above ground

Between every collector and collector subgroup there are non-insulated stainless steel pipes, see **1** and **2** in Figure 3, and between every group there is a combination of a non-insulated stainless steel pipe and a metal hose that connects the groups, see **2** in Figure 3. For every group there are also two underground pipes, one pipe taking in cold fluid and the other delivering hot fluid, see **3** in Figure 3.

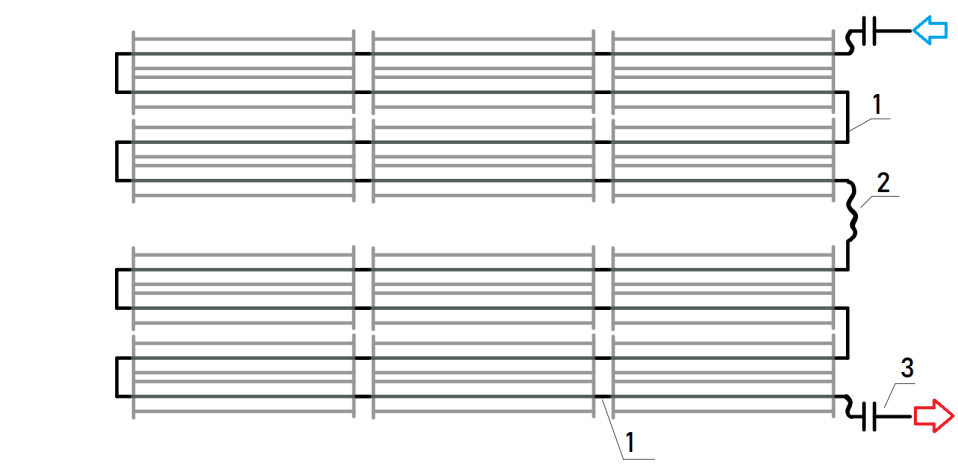

Figure 3: Collector group in Phase 1. **1**: Non-insulated stainless-steel pipe. **2**: Non-insulated stainless steel pipe and metal hose. **3**: Underground pipe.

2.2.2 Underground pipes

There are two grids of underground pipes, one delivering cold fluid to the collectors and one taking the hot fluid from the collectors to the heat exchanger. The piping system that takes the hot fluid from the collectors to the district heating can be seen in Figure 4 with connections to the collectors, heat exchanger, and which type of pipes are used.

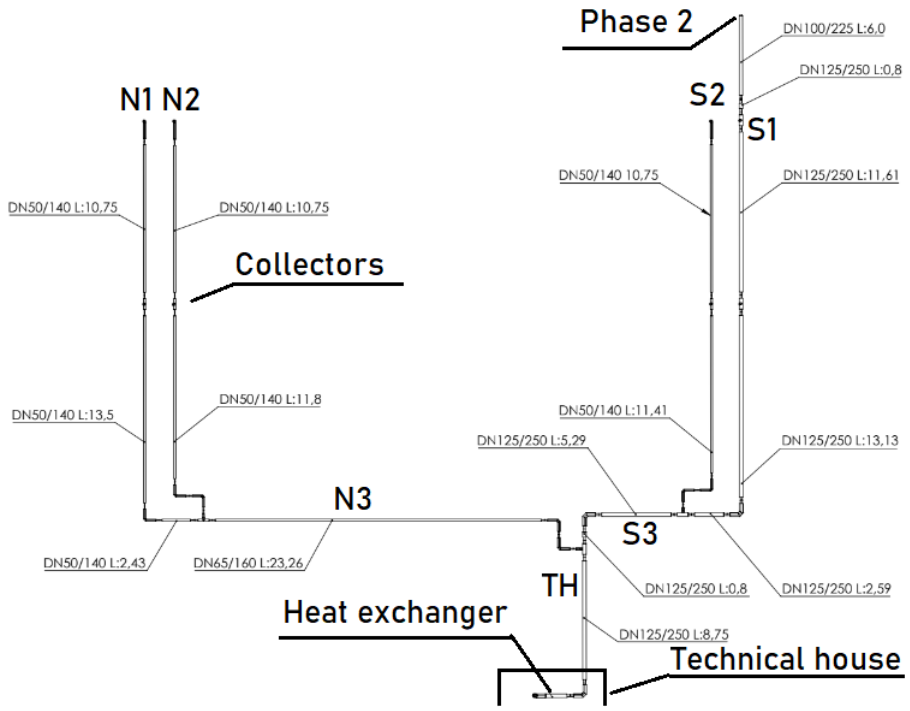

Figure 4: Approximate system figure of hot fluid underground pipes from collectors to heat exchanger.

Table 2 describes the different pipes in Figure 4 in more detail with their location, length, and nominated flow.

Table 2: Pipe location in Figure 4, pipe type, length, and nominated flow for all the pipes that delivers hot fluid to the heat exchanger.

Location	**Type**	**Length [m]**	**Nom. flow [m^3/h]**
S1	DN125/250	27.3	4.6
S2	DN50/140	22.2	4.6
S3	DN125/250	6.1	9.2
N1	DN50/140	26.7	4.6
N2	DN50/140	22.6	4.6
N3	DN65/160	23.3	9.2
TH	DN125/250	10.9	18.4

2.2.3 Sensors to measure temperature, flow, and pressure

To calculate the performance of the collector field it is necessary to measure temperature, flow, and pressure. Fluid temperature sensors are installed at three locations, directly after the collector groups, directly before the heat exchanger, and directly after the heat exchanger. For the temperature sensors of the fluid, two sensors are installed directly after each other to increase the accuracy of the data collection. Ambient air temperature is measured on the roof of the technical house. Pressure sensors and flow sensors are placed in the technical house directly before the heat exchanger.

3 Method

3.1 Data gathering, tools, and computer models

Data was collected at the solar thermal park by Absolicon, for example: solar irradiance, wind speed, water flow, and temperatures. The dates that was used in the models were those when all of the sensors were working correctly according to Absolicon, 2022-06-17:2022-08-11, 2022-08-16:2022-08-21, and 2022-08-26:2022-09-12. Performance data and specifications of the collector Absolicon T160 was gathered from Solar Keymark's certified database, see Table 1.

Python was used as the program to handle all of the data, calculate the different models and present the results. To understand the results better visual representations was made by plotting the calculated data with hourly averages. To make this process easier libraries (pre-written code) such as Matplotlib, NumPy, and Pandas, was used. Pandas was used to handle, change and analyze the data, while NumPy is a powerful tool to use for calculations on the data, and Matplotlib was used to visualize important data in 2D graphs. For those interested, see Appendix A for the developed models in Python.

3.2 Previous models

E. Magnusson's and RISE's previous research and models on performance evaluation was used as a foundation for this master's thesis. Their performance model was derived from an older ISO standard, ISO 9806:2017 [15]. The estimated performance was based on performance data from Solar Keymark, see Table 1, and sensor measurements calculated by

$$\begin{aligned}\dot{Q}_{estimate} =& A_{GF} * \big[\eta_{0,b} K_b(\theta_L, \theta_T) G_b + \eta_{0,b} K_d G_d - a_{1,\Delta Q}(T_m - T_a) - \\ & T_{\Delta Q}(T_m - T_a)^2 - a_5(dT_m/dt)\big]\end{aligned} \tag{1}$$

A model for calculating measured performance by using simple thermodynamics was also developed and was reused in this master's thesis [8].

$$\dot{Q}_{Measured} = v * C_p * \rho * (T_{out} - T_{in}) \tag{2}$$

where v, is the flow rate inside the pipes, T_{in} and T_{out} are the temperature before and after the heat exchanger, ρ the density of the fluid, and C_p the specific heat capacity.

3.3 Further development ISO

The performance calculation and filter was altered due to the new release of the ISO 24194:2022. In the new release of ISO 24194:2022 restrictions on operating conditions, such as shadows and wind velocity was added, an addition of a safety factor to the estimated performance calculations was also added.

3.3.1 New filter

Due to the fluctuation in sun hours and radiation throughout the year specific conditions are set to keep results valid. These conditions can be seen in Table 3 and are the basis of the filter.

Table 3: Conditions to be met when calculating estimated performance stated by the ISO 24194:2022.

Operation condition	**Limits**
Shading	No shading
Change in collector mean temperature	$\leq$ 5 K
Ambient temperature	$\geq$ 5 °C
Wind velocity	$\leq$ 10 m/s
G_b	$\geq$ 600 W/m^2

Mean temperature, ambient temperature, wind velocity, and G_b was measured by sensors. The requirement of no shading was modeled with solar angles and a new formula was introduced in the ISO 24194:2022. The formula used for calculating the height of a shadow due to internal shading from another collector was given by

$$H_{sh} = max\{0; min(w\left(1 - \frac{S}{P_y}\right); w)\} \tag{3}$$

where H_{sh} is the height of the shadow on the collector, w the width of the collector, S the spacing center between two adjacent rows, and P_y the coordinate of point C on the y-axis, see Figure 5 for a visual representation of the parameters.

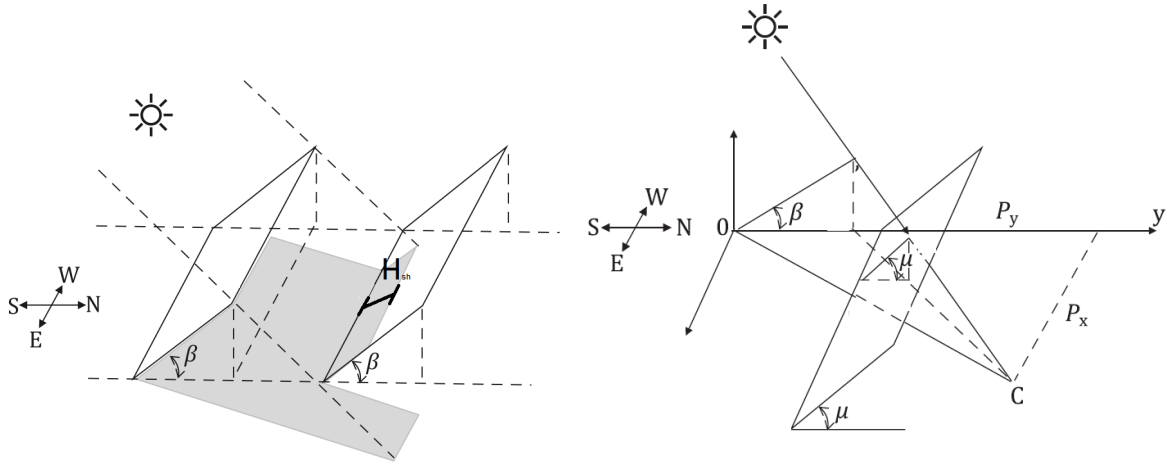

(a) **(b)**

Figure 5: Shadows due to internal shading from another collector [7]. **(a)** The shadow height is represented with H_{sh}. **(b)** Coordinate system for calculating point P_y.

H_{sh} was used to check how much of the collector is shaded and to check when there is no internal shading, $H_{sh} = 0$. For those interested, theory about solar angles and derivation of the calculated shading is given in Appendix C.2 and Appendix C.3.

3.3.2 Estimating performance

In the new ISO 24194:2022, the estimated performance is calculated with the addition of a safety factor, f_{safe}.

$$\begin{aligned}\dot{Q}_{estimate} =& A_{GF} * \big[\eta_{0,b} K_b(\theta_L, \theta_T) G_b + \eta_{0,b} K_d G_d - a_{1,\Delta Q}(T_m - T_a) - \\ & T_{\Delta Q}(T_m - T_a)^2 - a_5(dT_m/dt)\big] * f_{safe}\end{aligned} \tag{4}$$

where f_{safe} is based on three levels of accuracy. The safety levels are based on requirements on measurements and sensors. Level I grants a safety factor of 0.95 and level II - III gives a safety factor of 0.9, see Appendix D.1 for a detailed description of the requirements. A higher safety factor yields more accurate and better results but the drawback is more expensive equipment and time invested. The ISO 24194:2022 also presents a more accurate way of calculating the safety factor, which was the method used.

$$f_{safe} = f_P * f_U * f_O \tag{5}$$

f_P, relates the heat losses from pipes in the collector loop to the useful heat.
f_U, relates the uncertainties in measurement to the produced heat.
f_O, relates other non-ideal conditions such as non-ideal flow and uncertainties in the model.
The safety factor was not calculated with f_O in the main calculations due to no accurate

methods of calculating other losses. f_U was based on the previously mentioned safety levels where the sensitivity of the sensors was investigated and engineers at Absolicon was questioned about their maintenance routine. f_P was calculated with methods calculating heat losses from pipes stated in the ISO 24194:2022 and comparing the total heat losses to the estimated power.

3.3.3 Heat losses in pipes, ISO

ISO 24194:2022 presented a simplification of heat losses in a pipe system based on empiric values. The heat losses from pipes was estimated by

$$\dot{Q}_{pipe,d} = q_{1-pipe} * L_{pipe} * (\bar{T}_m - \bar{T}_a) \tag{6}$$

where q_{1-pipe} represents the empirically derived specific heat losses factor per m pipe and volume, L_{pipe} the length of the pipes, $\bar{T}_m$ is the average temperature inside the pipe, and $\bar{T}_a$ the average ambient temperature. q_{1-pipe} is calculated by

$$q_{1-pipe} = 0.32 * \left(\frac{V_{pipe}}{L_{pipe}} \right)^{0.22} \tag{7}$$

where V_{pipe} is the volume of the pipe, and the factor 0.32 and the power of 0.22 is empirically derived by the ISO.

3.3.4 Comparing estimated and measured performance

After calculating the heat losses and f_p the estimated power production was calculated with f_{safe}. When the estimated power and measured power was calculated a comparison between them was made. Three different comparison models was used and stated in the ISO 24194:2022 [7]. First, the solar field performance is verified when the measured power is greater or equal to the estimated power for 20 consecutive points. Secondly, the relationship of the measured and estimated power was and should be plotted with a scatter plot and linear relationship plot to check for derivation and consecutive points. An example plot for valid data points is shown in Figure 6.

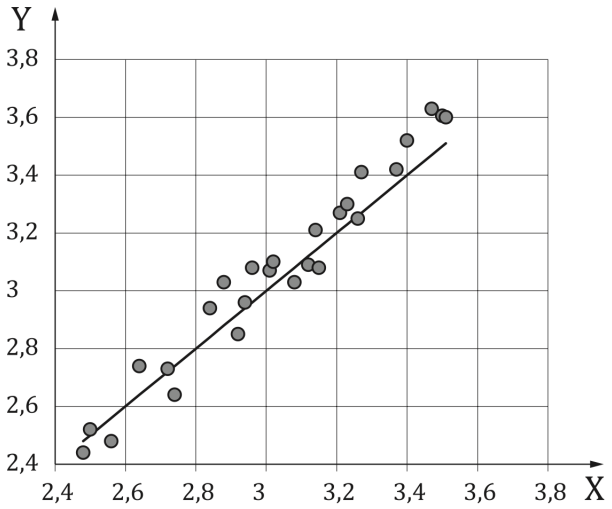

Figure 6: Example plot of measured and estimated power production [7]. **X-axis:** estimated power. **Y-axis:** measured power.

Lastly, the average hourly estimated power and the average hourly measured power was and should also be compared to verify the solar thermal field, where the average measured power should be larger than the estimated power. A visual representation of the comparison between average hourly measured and estimated power can be seen in Figure 7.

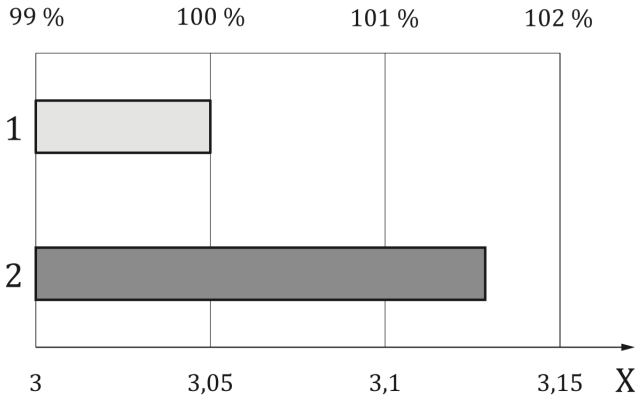

Figure 7: Example figure of average hourly measured and estimated power [7]. **X-axis:** average power for valid points. **Y-axis:** 1. Estimated power. 2. Measured power.

3.4 Sensitivity analysis of ISO

Changes to the parameters of the ISO 24194:2022 was made to see how different scenarios changed the performance evaluation. First, f_{safe} was looked into due to f_{safe} not being clearly defined, it could be based solely on the safety levels mentioned before or be calculated with heat losses and uncertainties in measurements, sensors, flow-rate, the models,

etc. Therefore three different scenarios for f_{safe} was made. First, by calculating heat losses for a general case using thermodynamics a new f_p was calculated. Secondly, with different uncertainties for measurements, f_U, for the safety levels: Level I => $f_U = 0.95$, and Level II & Level III => $f_U = 0.9$. And lastly with approximations for f_O. After the safety factor was investigated irradiance, daily performance, and a "real-world" scenarios were explored. Where the real-world scenario was estimated by simulations of observing the behavior of the solar field when there was no filter.

3.4.1 Safety factor sensitivity, f_p

To calculate the new f_p, three new models based on thermodynamics for heat losses was made: heat losses in pipes above ground, pipes underground, and the impact of wind speed.

3.4.2 Heat losses in pipes above ground

The pipes above ground was modeled with and without insulation where steady-state was assumed in temperature and flow. A figure representing the two pipes, with insulation and without insulation, is shown in Figure 8.

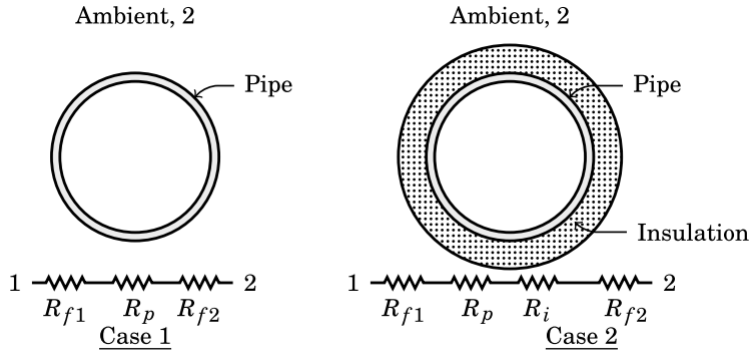

Figure 8: Cross sections of two pipes. To the left: a pipe without insulation. To the right: a pipe with insulation [16]

.

The total resistance due to conduction and convection can be modeled as resistances in series, see Figure 8. The film resistance R_{f1} is negligibly small relative to the other resistances, hence it is reasonable to ignore in the total resistance [16]. The total resistance ***without insulation*** [16] is given by

$$R_{totalWithoutInsulation} = R_p + R_f = \frac{1}{2\pi\lambda_p} ln\left(\frac{r_o}{r_i}\right) + \frac{1}{2\pi r_o h} \tag{8}$$

where R_p is the conduction resistance, R_f is the convection resistance, λ_p is the thermal

conductivity of the pipe, r_o is the outer radius, r_i the inner radius, and h the convective heat transfer coefficient of air. The total resistance ***with insulation*** [16] is

$$R_{totalInsulated} = R_p + R_i + R_f = \frac{1}{2\pi\lambda_p} ln\left(\frac{r_2}{r_i}\right) + \frac{1}{2\pi k_i} ln\left(\frac{r_o}{r_2}\right) + \frac{1}{2\pi r_o h} \tag{9}$$

where r_2 is the outer radius of the inner pipe, and R_i is the conduction resistance of the insulation.

The ***total heat losses*** [16] was then calculated by

$$Q_{total} = L_{pipe} \frac{T_m - T_a}{R_{total}} \tag{10}$$

using the relevant resistance calculated with Equation 8, or Equation 9, where Q_{total} is the total heat losses. See Appendix C.4 for the derivation of the resistances.

3.4.3 Heat losses in underground pipes

For underground pipes, the added complexity of thermal conductivity in the ground and a thermal field due to the parallel cold pipe is included. Figure 9 shows the configuration and parameters between the supply and return pipe.

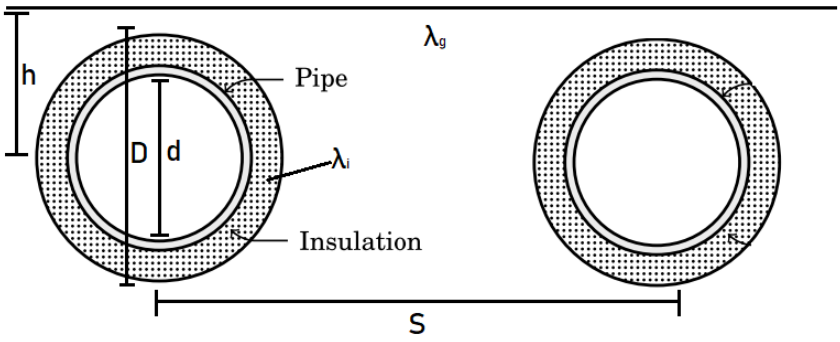

Figure 9: Supply and return pipe with measurements [17].

To calculate the heat losses from underground pipes the principle of adding resistances still applies but in this case with added ground resistance and a relative temperature field due to interference between the temperature between the two pipes [17]. The heat loss in a singular supply pipe [17] was calculated by

$$Q_{pipeGround} = L_{pipe}\pi d\frac{(R_g + R_i) * (T_s - T_a) - R_c * (T_r - T_a)}{(R_g + R_i)^2 - R_c^2} \tag{11}$$

where the different resistances [17] are given by

$$R_i = \frac{d}{2\lambda_i} * ln\left(\frac{4h}{D}\right) \tag{12}$$

$$R_g = \frac{d}{2\lambda_g} * ln\left(\frac{4h}{D}\right) \tag{13}$$

$$R_c = \frac{d}{2\lambda_g} * ln(((2h/s)^2 + 1)^{0.5}) \tag{14}$$

where R_i is the conduction through the insulated pipe, R_g the conduction through the ground, and R_c is due to the thermal field interference with the nearby colder return pipe [17].

3.4.4 External heat transfer coefficient

Heat losses due to the external heat transfer coefficient of air was also calculated and modeled to see how the heat losses would vary throughout the day. The formula used to model heat losses from pipes due to wind speed [18] was

$$h_{air} = (0.15 + 0.182 * \sqrt{v_{wind}}) * (98 - T_a) \tag{15}$$

where h_{air} is the convective heat transfer coefficient of air, v_{wind} wind speed, and T_a ambient temperature. h_{air} was used as h in Equation (8) and Equation (9).

3.4.5 Safety factor sensitivity, f_O and f_U

First, the model of changing f_U was made, with Safety Level I, $f_U = 0.95$ and Level II & Level III, $f_U = 0.9$. Secondly, due to f_O not being easily accurate quantified the models was made on educated guesses in f_O, where mainly malfunction of the tracking system and non-ideal flow was considered.

3.4.6 Irradiance sensitivity

Since Sweden does not have high direct normal irradiation, and even less in northern Sweden, it is interesting to change the limit of G_b in Table 3 to a lower value. Three different models for direct irradiance limits were made: G_b of 400 W/m^2, 500 W/m^2, and 600 W/m^2.

3.4.7 Daily performance analysis

A performance model for a day where the conditions were mostly met was plotted for estimated and measured power output. A model for color grading the measured and performance comparison based on valid data and hours was also made to see how the valid data points varied over the day.

3.4.8 Real world analysis

Estimated safety parameters based on a real-world scenario where the filters are removed are presented. The uncertainty in measurements, f_U, was set to $f_U = 0.925$ since that even though the sensors was not maintained properly the solar thermal park had installed accurate measurement sensors. f_p was estimated to be a bit higher due to the losses in start-up which is not considered in the steady-state condition, $f_p = 0.95$. f_O was set to, $f_O = 0.98$ due to estimations on malfunctions on the tracking system and non-ideal flow. Finally, multiplying f_p, f_O, and f_U, giving $f_{safe} = 0.86$. The results were then modeled according to the verification methods of the ISO 241941:2022 and the daily performance model.

3.4.9 Applying suggested improvements

By analyzing the results of the heat losses and daily performance two suggestions to improve the performance of the solar thermal park was made. The suggestions were to insulate the pipes above ground, and investigate and possibly fix the solar tracking system. Further analyzing the models in heat losses and daily performance the increase in performance was calculated. By applying the increased performance in measured power output the standard ISO evaluation, mentioned in Section 3.3.4, was used to evaluate the improved system.

4 Results

4.1 Implementing the new ISO model

The results in this section represent the improved methods to verify the performance at Högslätten Solar Thermal Park based on the specified requirements, see Table 3, and comparison methods stated in the ISO 24194:2022.

4.1.1 New filter

Before applying the condition filter based on the conditions stated in Table 3, internal shading between the collectors needs to be modeled using Equation 3. The results of plotting the shadow height for a day in the middle of June can be seen in Figure 10.

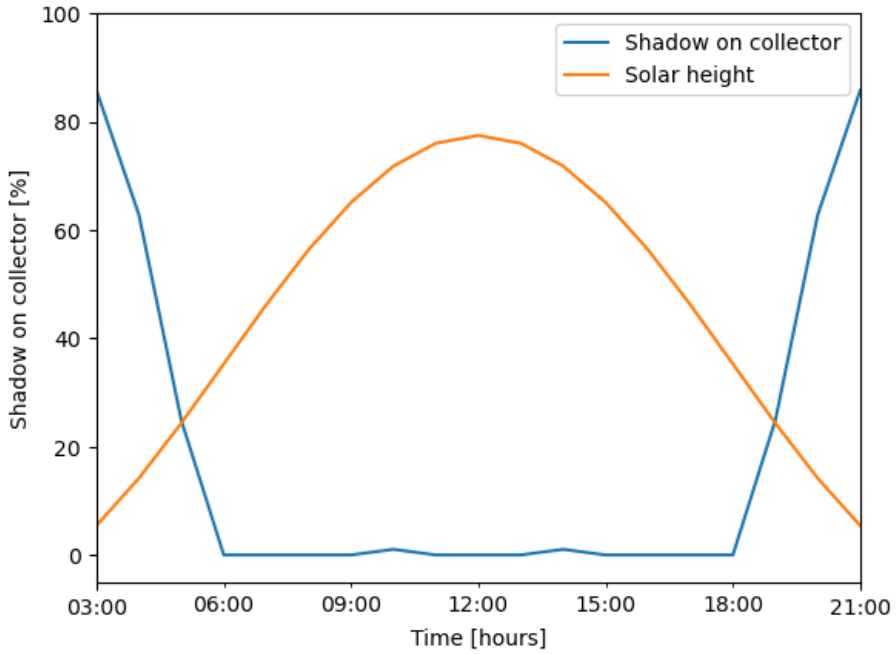

Figure 10: Amount of internal shadows on a collector and the solar height throughout a day in the middle of June.

For this specific day, it can be seen that there are no shadows between 06:00 - 18:00 besides two small bumps between the hours 9:00 - 12:00 and 12:00 - 15:00.

The results of filtering the hourly data set with the specified requirement parameters: shadows, change in collector mean temperature, ambient temperature, wind velocity, and beam irradiation, according to Table 3, can be seen in Figure 11.

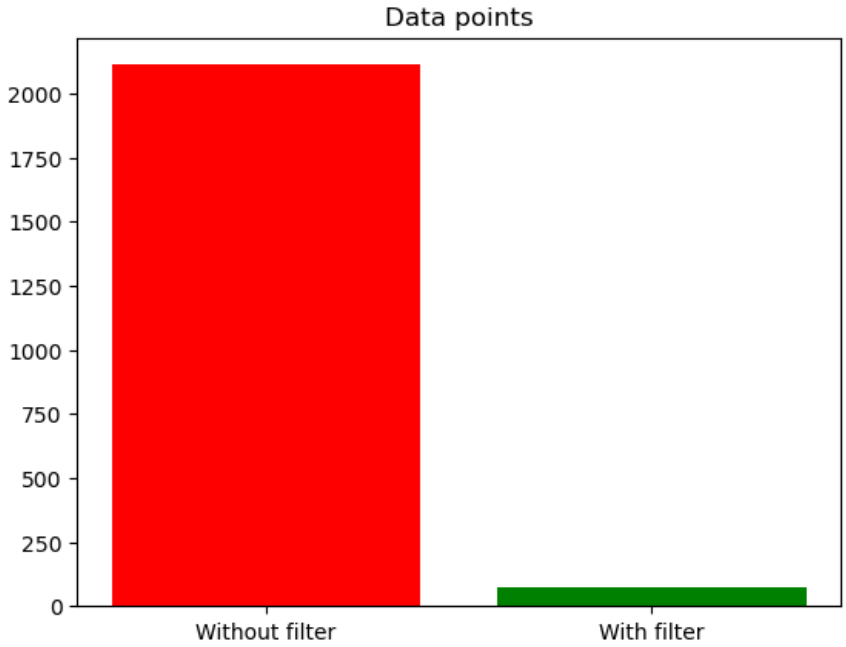

Figure 11: Filtered and non-filtered data points. To the left: all of the original data points. To the right: all of the valid data points according to the ISO 24194:2022.

A drastic decrease in data points can be seen after applying the filter, left with around 100 valid data points, approximately dismissing 95% of the original data set.

4.1.2 Estimating performance

To determine the heat loss factor, f_p, the total heat losses first needs to be calculated. The results from calculating the total heat losses from underground pipes and pipes above ground using Equation 6 can be seen in Figure 12.

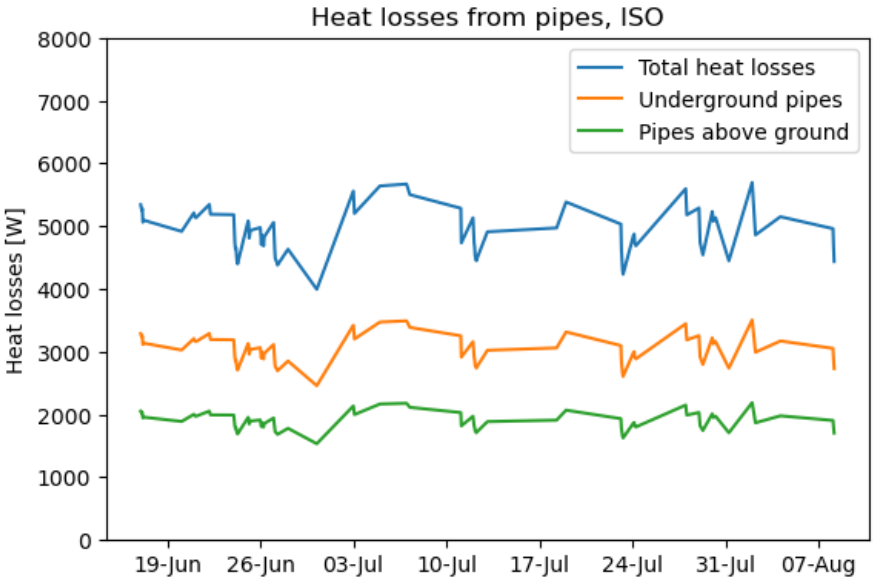

Figure 12: Total heat losses from underground pipes and pipes above ground in hourly averages, calculated for all valid data points.

In Figure 12 it can be seen that the total heat losses are approximately 5000 W throughout the summer days, with some fluctuation. There is also a decisive drop and increase in heat losses around between 26-Jun and 03-Jul. With the calculated total heat losses the heat loss factor, f_p, was calculated by dividing the heat losses with the estimated power, the results can be seen in Figure 13.

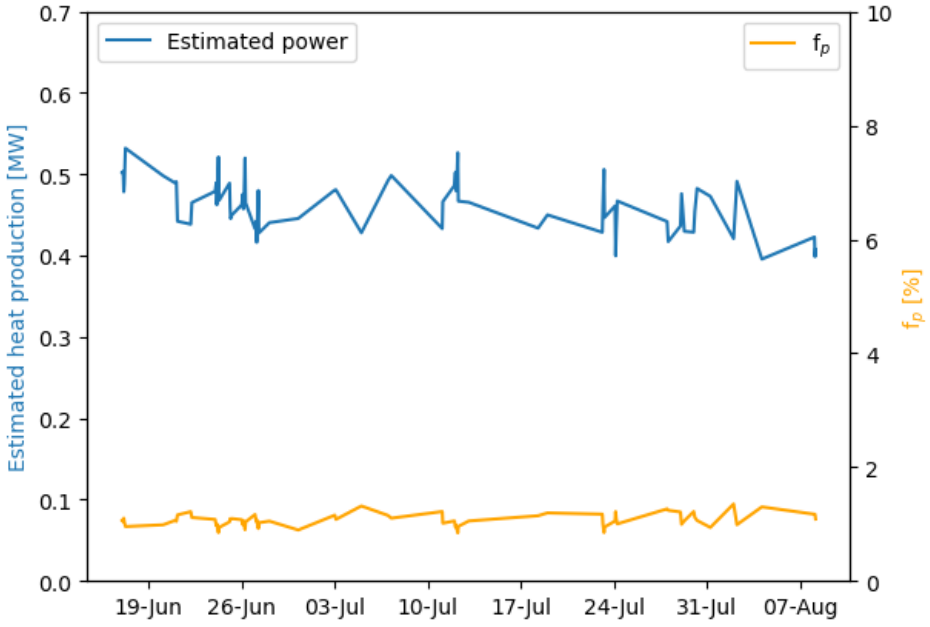

Figure 13: The upper line represents the estimated power production before adding the safety factor. The lower line is the heat loss factor, f_p based on the total heat losses and estimated power.

It can be seen in Figure 13 that the total heat losses are just a fraction of the estimated power production, meaning the heat loss factor is very low. By looking at the graph the heat loss factor is approximated to around 1%, $f_p = 0.99$.

4.1.3 Estimated vs Measured

Before comparing the estimated and measured power the safety factor, f_{safe}, must be added to the estimated power. The resulting safety factor, $f_{safe} = 0.89$ due to the parameters f_p, f_U, and f_O, $f_p = 0.99$, calculated with the total heat losses. The thermal park got a safety level of III due to not cleaning the sensors frequently enough, $f_U = 0.9$. Lastly, $f_O = 1$ due to no way of accurately calculate non-ideal flow or other losses. The results of the estimated and measured power for all the valid data points are presented in Figure 14.

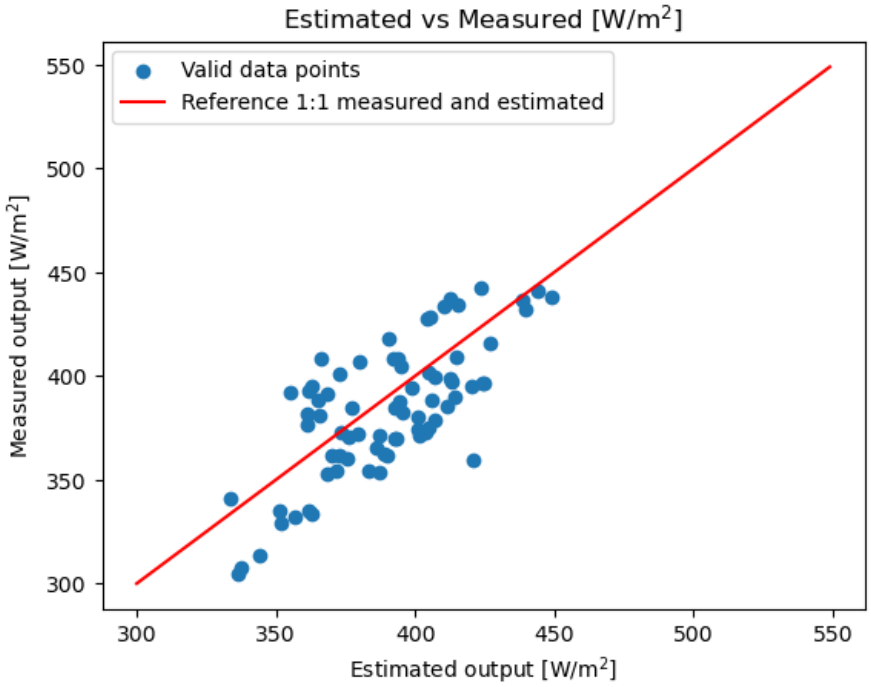

Figure 14: The data points represent the valid measurements for estimated and measured output with $f_{safe} = 0.89$. The linear line represents the 1:1 relationship between estimated and measured power.

There are not any major deviations in Figure 14, though a minor deviation can be seen at 425 W/m^2 estimated output and 350 W/m^2 measured output, which could be due to a malfunction of the solar thermal park. More importantly, there are not twenty consecutive data points where the average measured power is equal to or greater than the average estimated power, which is a requirement for verification of the solar thermal park performance according to the ISO 24194:2022.

Another requirement for verification of the solar thermal park was that the average hourly measured power should be higher or equal to the hourly average estimated power. A representation of the hourly average measured and estimated power with the same safety factor as before can be seen in Figure 15.

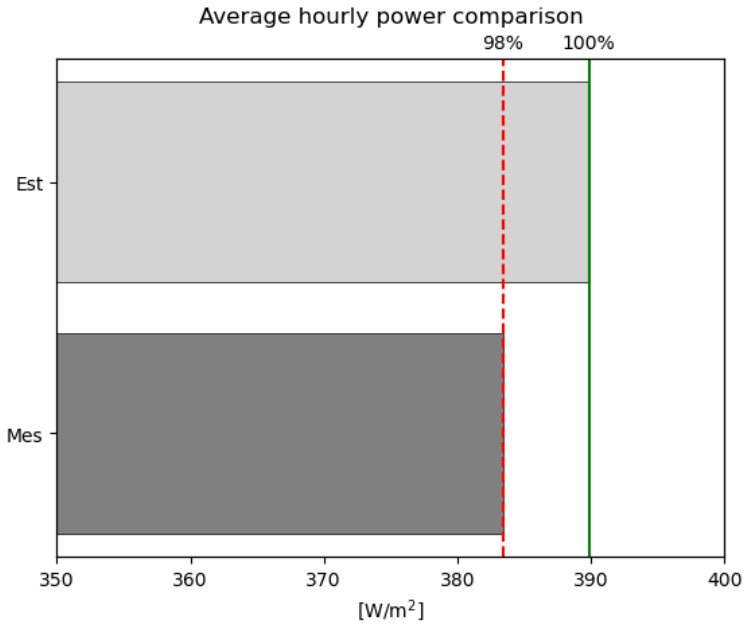

Figure 15: The average hourly power production. The upper bar-plot is the estimated power production with $f_{safe} = 0.89$. The lower bar-plot is the measured power production.

The solar thermal field is not verified according to Figure 15 since the hourly average measured power is lower than the hourly average estimated power.

4.2 Sensitivity analysis

The results of changing the parameters: f_p, f_O, f_U, and irradiance is given in this section. An analysis of daily performance and a real-world scenario is also presented.

4.2.1 Safety factor sensitivity, f_p

In this section, the heat loss factor, f_p, was instead modeled with total heat losses calculated by general thermodynamics. In order to determine the heat losses the dependence of wind speed was modeled without insulation and with different-sized insulation of polyurethane foam. The results can be seen in Figure 16.

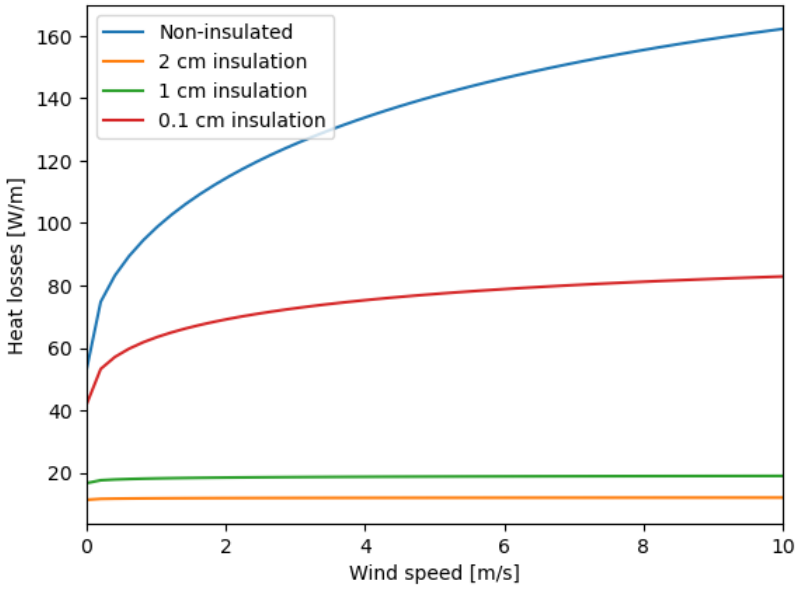

Figure 16: Impact of wind velocity on the heat losses from pipes above ground for 0 - 10 m/s wind speeds with different sizes of insulation: 0 cm, 0.1 cm, 1 cm, and 2 cm.

Figure 16 shows that the dependence on wind speed drastically decreases with just a little insulation. It is also evident that for poor or no insulation the heat losses are increasing drastically in the beginning, following the form of a square root function. The results of calculating the total heat losses for three different scenarios, ISO estimations Equation 6, and two general cases, without insulation Equation 8, and with insulation Equation 9, can be seen in Figure 17.

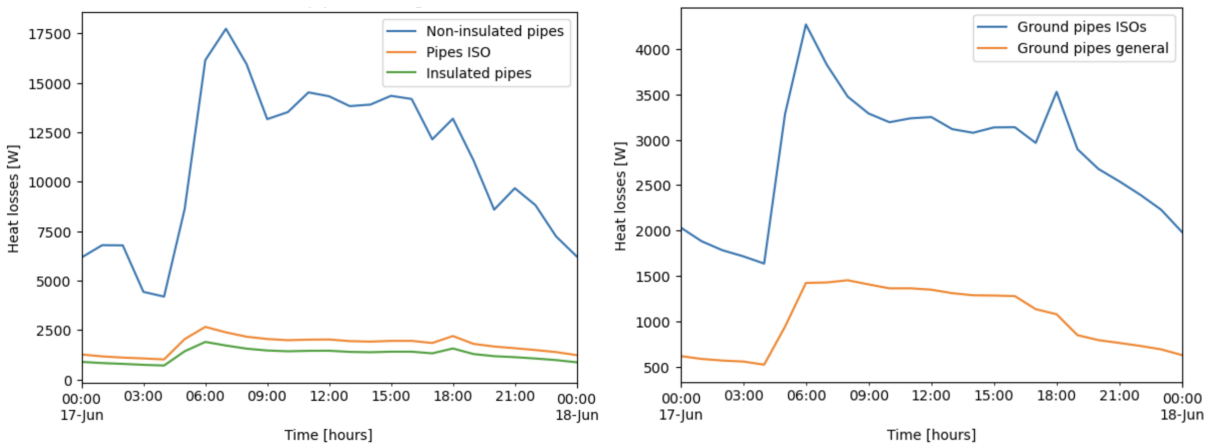

(a) **(b)**

Figure 17: Heat losses modeled over a day. **(a)** Heat losses from pipes above ground modeled with ISO estimations and the general formula for insulated and non-insulated pipes. **(b)** Heat losses from underground pipes modeled with ISO estimations and the general formula.

Figure 17a shows that the heat losses calculated with ISO and insulated pipes are similar

throughout the day while the heat losses from non-insulated pipes are relatively high and fluctuate a lot during the day. Figure 17b shows an inverted relationship, the calculations on heat losses in the underground pipes with ISO estimations are higher throughout the day relative to the general calculation for underground pipes.

The results of calculating the total heat losses for two different scenarios, with ISO estimations and the general case can be seen in Figure 18.

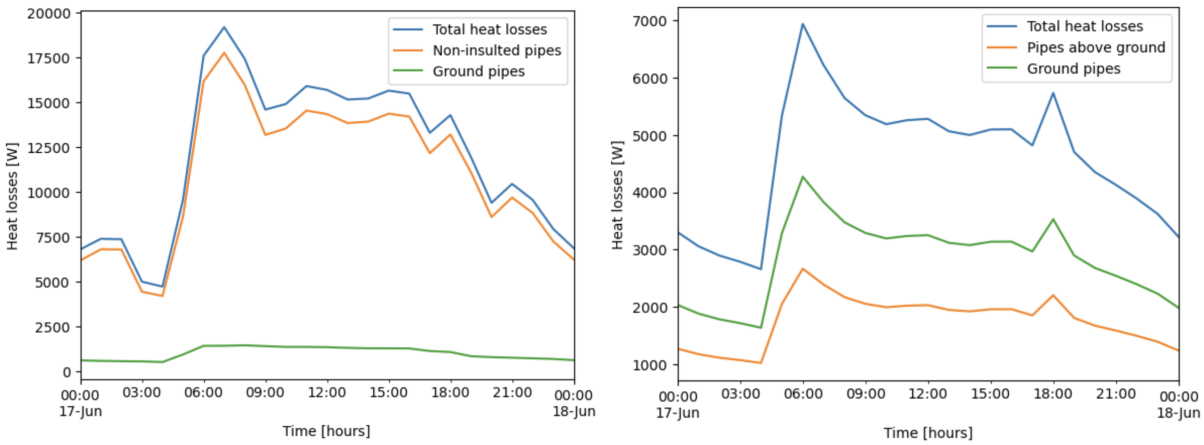

(a) **(b)**

Figure 18: Total heat losses modeled over a day. **(a)** Total heat losses modeled with the general formula for non-insulated pipes above ground and underground pipes. **(b)** Total heat losses modeled with ISO estimation formula for pipes above ground and underground pipes.

Figure 18a shows that heat losses from pipes modeled with the general equations are for the most part due to heat losses from the non-insulated pipes. Figure 18b shows that the heat losses from underground pipes are approximately double the amount from pipes above ground but the difference is still not as large as in Figure 18a. Relative to the estimated heat production the total heat losses in Figure 18a are three percent, and in Figure 18b one percent.

4.2.2 Estimated vs Measured

The estimated power can now be calculated by implementing f_{safe}. After comparing the total heat losses to the estimated power production the heat losses are 3%, $f_p = 0.97$. As mentioned before, due to not cleaning the sensors frequently enough the solar thermal park gets a safety level of III, $f_U = 0.9$ and $f_O = 1$ due to uncertainty in magnitude.

Instead of applying the safety factor directly to the valid data points the safety factor was applied to the linear line, divided into heat losses and uncertainties in measurements where heat losses are added as a constant value and uncertainties in measurments and other losses are added as a safety margin. This can be seen in Figure 19.

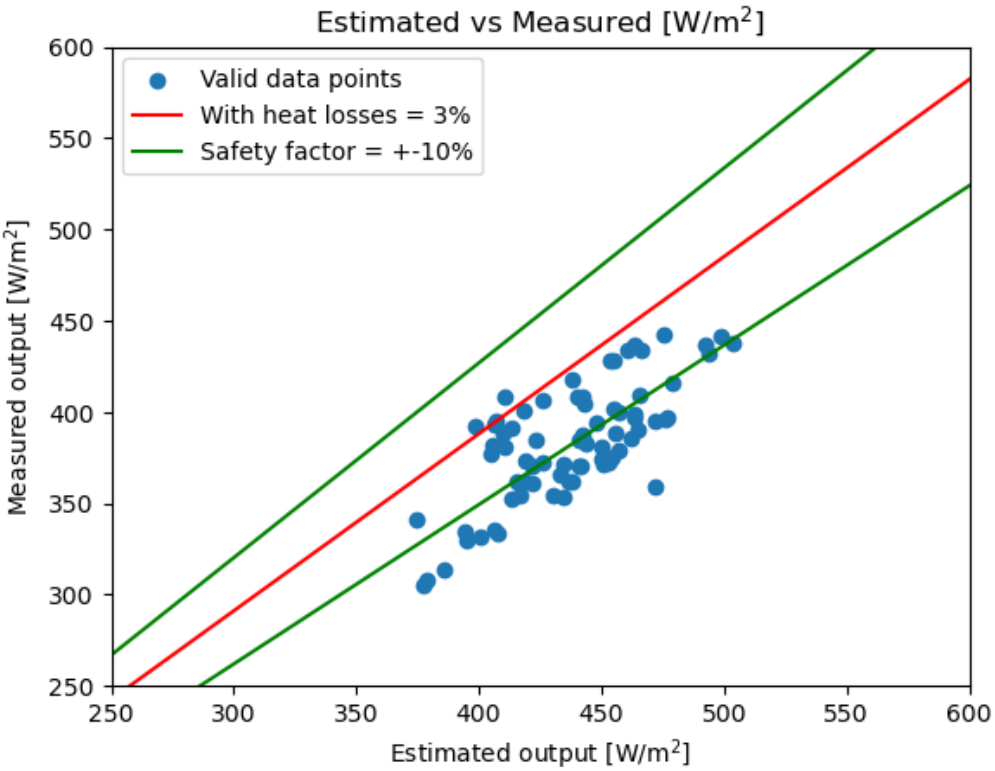

Figure 19: The data points represent the valid data points for measured and estimated output. The red linear line represents the 1:0.97 relationship between measured and estimated, due to $f_p = 0.97$. The green lines represent the safety factor, due to uncertainties in measurements, $f_U = 0.9 = +\text{-}10\%$.

In Figure 19 one can see that the more data points are verified relative to the previous comparison figure, Figure 14, a few data points are above the red line representing f_{safe} with heat losses and even more are over the bottom line, representing the f_{safe} lower limit.

To verify the result the average hourly measured power is compared with the average estimated power. This can be seen in Figure 20.

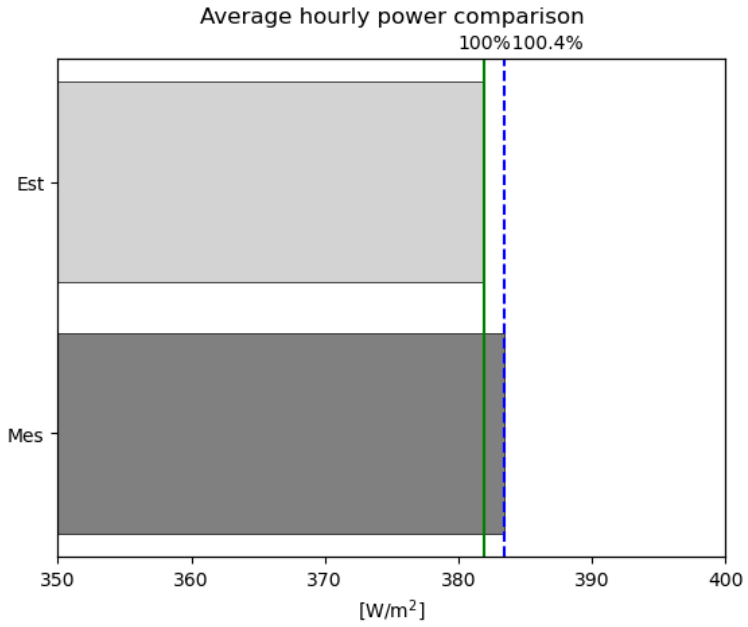

Figure 20: The average hourly power production for measured and estimated calculations with $f_p = 0.97$ and $f_U = 0.9 => f_{safe} = 0.873$.

The average estimated power production was 383 W/m^2 and the measured was 384 W/m^2, 0.4% higher. By more accurate calculated heat losses, the solar thermal park is verified according to the ISO 24194:2022.

4.2.3 Safety factor sensitivity, f_U and f_O

Due to the safety factor not being easily quantified this section represents the safety factor f_{safe} with differences in f_O and f_U, and keeping $f_p = 0.97$. First, the results of changing f_U are presented, safety level I gives $f_U = 0.95$ and Level II & Level III gives $f_U = 0.9$. The results can be seen in Figure 21.

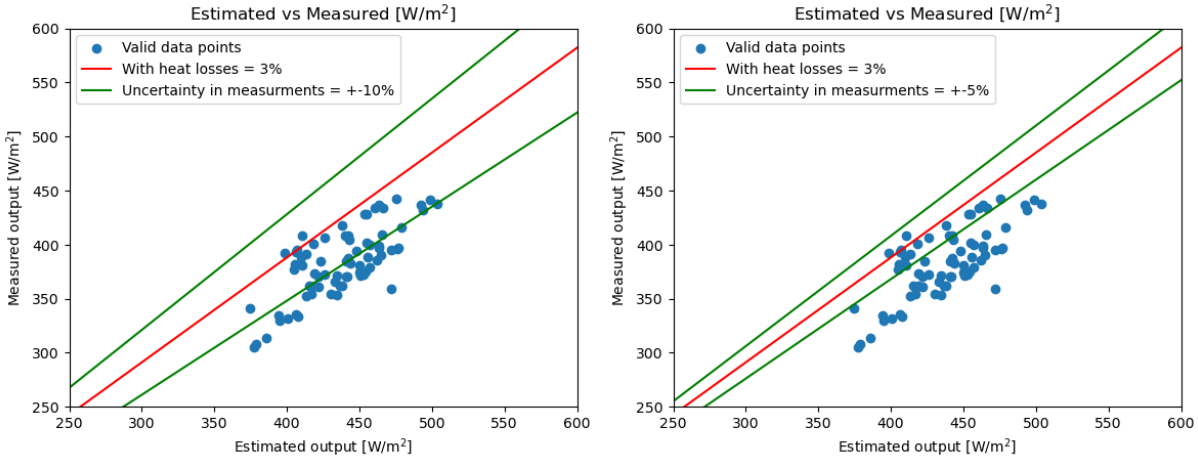

(a) **(b)**

Figure 21: The data points represent the valid data points for measured and estimated output. The red linear line represents the 1:0.97 relationship between measured and estimated due to f_p, heat losses in pipes. The green lines represent the safety factor due to uncertainties in measurements. **(a)** $f_U = 0.9$. **(b)** $f_U = 0.95$.

In Figure 21 (a) approximately half of the data points are verified, and in Figure 21 (b) only around a third of the data points are verified. These results show that the safety level, Level I, Level II & Level III, of the solar thermal park has a large impact on the final verification limits.

Lastly, f_O is modelled as 1-2%, $f_O = 0.98$ and $f_O = 0.99$, mainly due to possible malfunction of the tracking system, not perfectly clean collectors, and non-ideal flow. The results of adding the f_O factor can be seen in Figure 22.

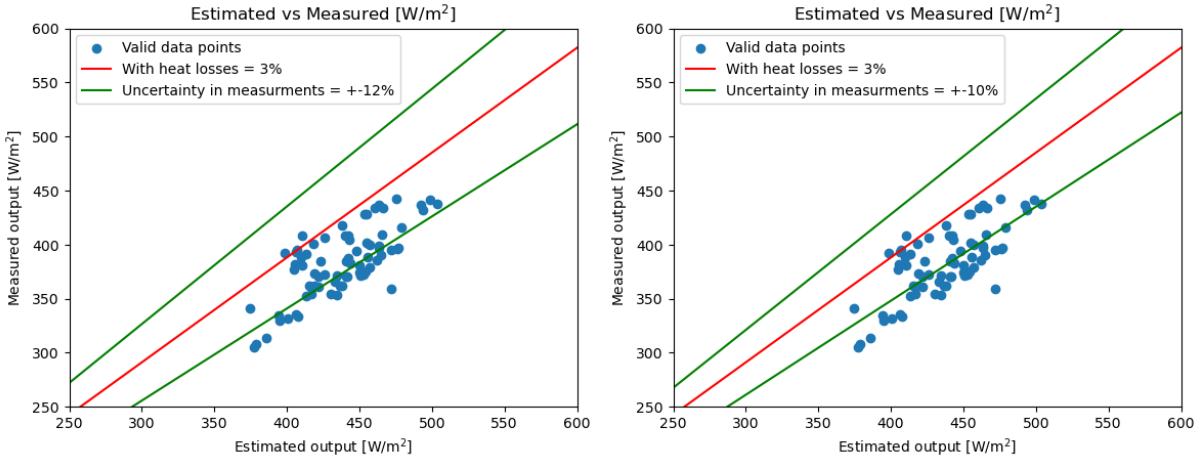

(a) **(b)**

Figure 22: The data points represent the valid data points for measured and estimated output. The red linear line represents the 1:0.97 relationship between measured and estimated due to f_p, heat losses in pipes. The green lines represent the safety factor due to uncertainties in measurements. **(a)** $f_p = 0.97$, $f_U = 0.90$, $f_O = 0.98 => f_{safe} = 0.86$. **(b)** $f_p = 0.97$, $f_U = 0.90$, $f_O = 1 => f_{safe} = 0.87$.

The results of adding the f_O factor are not major, which is expected with a maximum 2%, still, there are a few more verified data points in Figure 22 (b).

4.2.4 Irradiance sensitivity

Since northern Sweden does not have much direct sunlight, it is interesting to change the limit of G_b in the condition Table 3 to a lower value. Figure 23 shows the difference in valid data points for a lower limit of direct irradiance, G_b, of 400 W/m^2, 500 W/m^2, and 600 W/m^2 based on f_{safe} mentioned in the first comparison, $f_{safe} = 0.89$.

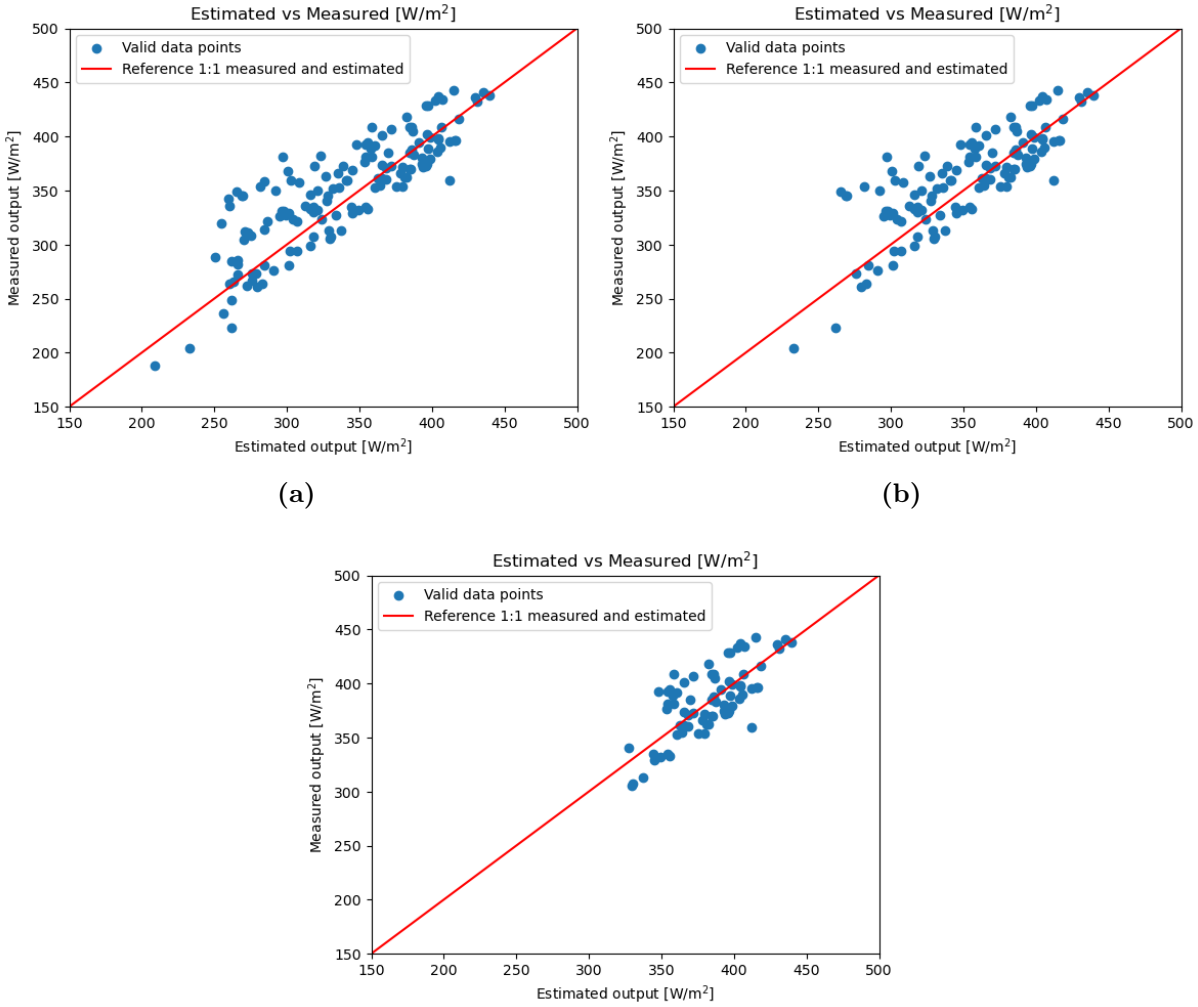

Figure 23: The valid data points represent measured and estimated output for three different scenarios of minimum direct irradiance, G_b. The red linear line represents the 1:1 relationship between measured and estimated output. $f_{safe} = 0.89$ applied to estimated data points. **(a)** $G_b = 400\ W/m^2$. **(b)** $G_b = 500\ W/m^2$. **(c)** $G_b = 600\ W/m^2$.

There are a lot more valid points for a) and b) in Figure 23, higher ratio data points over the 1:1 reference with lower direct irradiance, and the output is also a lot lower with lower direct irradiance. The lowest output is around 200 W/m^2 in measured in Figure 23 a) and the lowest in Figure 23 c) is 300 $\mathrm{W/m^2}$. How the lower output affects the average power is shown in Figure 4.2.4.

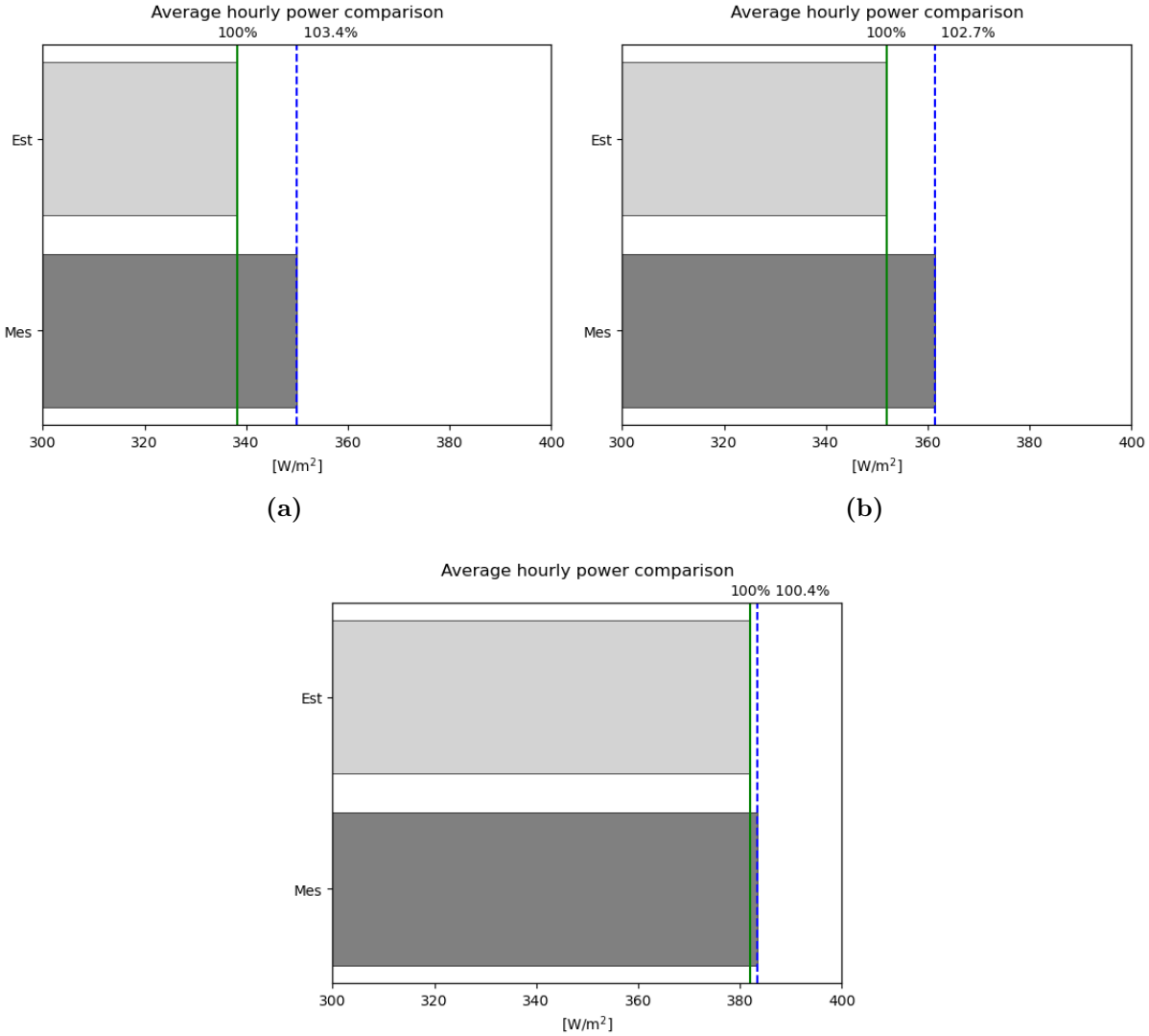

Figure 24: The average power production for three different scenarios of direct irradiance, G_b. **(a)** $G_b = 400\ W/m^2$. **(b)** $G_b = 500\ W/m^2$. **(c)** $G_b = 600\ W/m^2$.

It can be seen that the total average power for both estimated and measured is now lower in Figure for the cases (a) and (b), which is expected. However, the percentage difference between estimated and measured average power is now higher due to the higher measured power output relative to the estimated power output which could be seen in Figure 23.

4.2.5 Daily performance analysis

The results of the daily production for a day with valid data points between 9:00 - 15:00 can be seen in Figure 25.

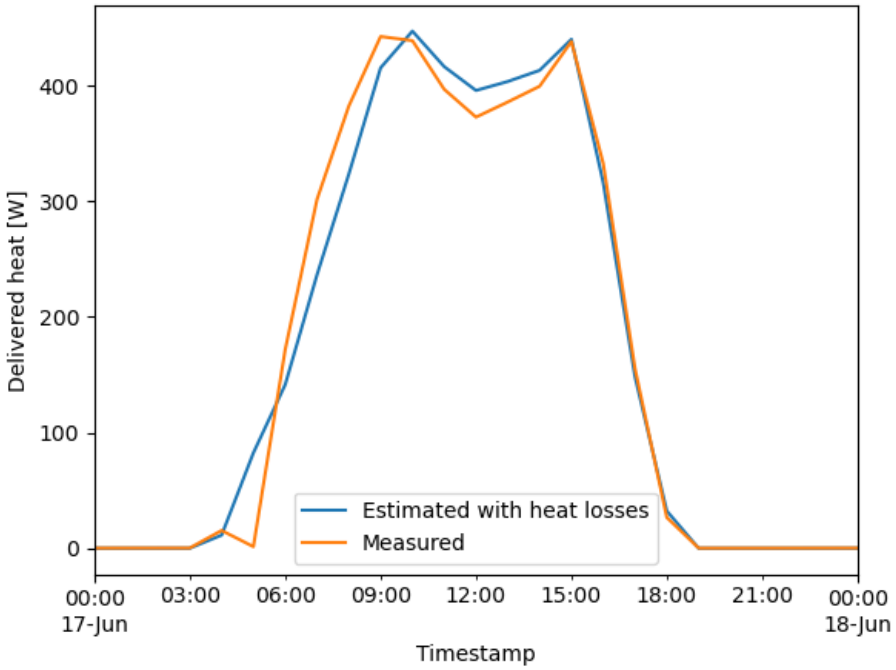

Figure 25: The performance in measured and estimated power for a day with valid data points between 9:00 - 15:00. $f_p = 0.97$ and $f_U = 0.9 => f_{safe} = 0.87$.

In Figure 25 one can see that estimated and measured power are quite similar. In the early morning, between 03:00 and 06:00 it can be seen that the measurement is a lot lower than estimated, due to the system starting cold, after 06:00 until just before 09:00 the measured spikes going beyond the estimated. In the middle of the day 09:00-15:00 a dip in measured and estimated performance can also be seen, where measured goes below estimated. The rest of the day measured and estimated are quite similar.

The results of adding a color gradient, where darker colors represent earlier hours, gradually shifting to lighter colors, to the original scatter plot, Figure 14, can be seen in Figure 26.

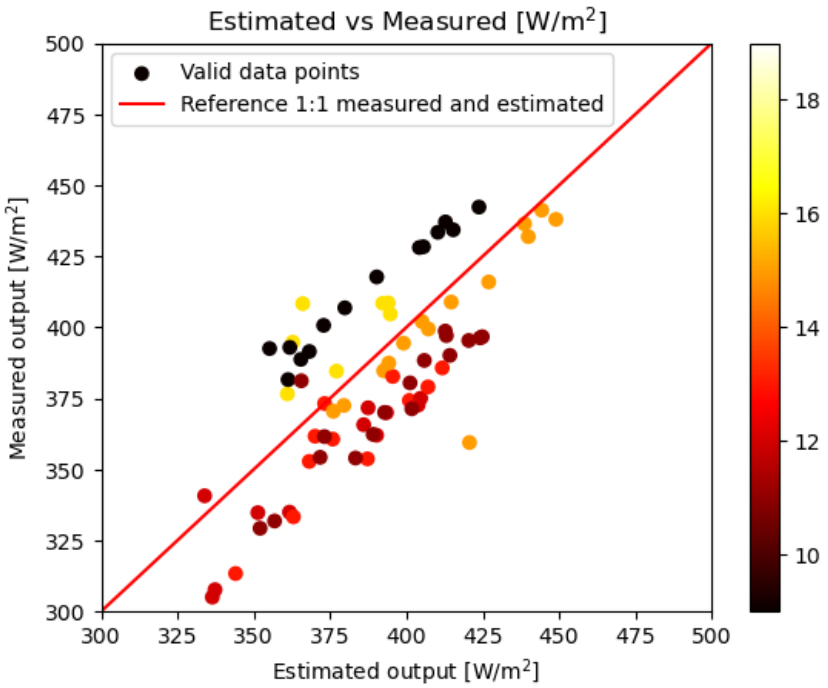

Figure 26: The data points represent the valid data points for measured and estimated output where darker colors are in the morning, gradually shifting to lighter colors in the evening. f_{safe} = 0.89.

In Figure 26 a pattern can be seen where the same hours for the different days line up similarly. The best measured vs estimated performance can be seen for the early hours of the day, hours 9 and 10, and worse calculated performance in the middle of the day, hours 11-14. The rest of the day is more spread out but in general around or above the margin. This also confirms that the pattern seen in Figure 25 is valid for all the days throughout the year. The pattern also makes the requirement of 20 consecutive points impossible.

4.2.6 Real-world analysis

The uncertainty in measurements, f_U, was set to $f_U = 0.925$ since even though the sensors was not maintained properly the solar thermal park had accurate measurement sensors. f_p was estimated to be a bit higher due to the losses in start-up which is not considered in the steady-state condition, $f_p = 0.95$. f_O was set to, $f_O = 0.98$ due to estimations on malfunctions on the tracking system and non-ideal flow. The results of estimated and measured performance using the "real world" parameters and color scaling can be seen in Figure 29.

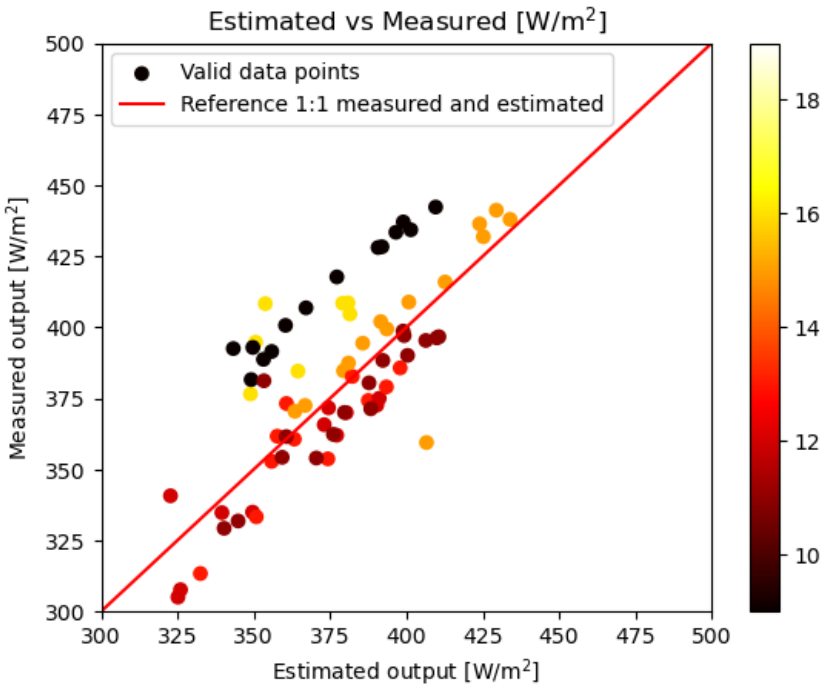

Figure 27: The data points represent the valid data points for measured and estimated output where darker colors are in the morning, gradually shifting to lighter colors in the evening. $f_O = 98$ $f_p = 95$ and $f_U = 92.5 => f_{safe} = 86$.

Examining Figure 27 it is obvious that the worst performance is around 12:00. For the other valid data points the measured performance is higher than the estimated. The measured output is also better than the estimated performance relative to only using parameters entirely based on the ISO 241941:2022, see Figure 14.

Using the same "real world" parameters the hourly average power production was modeled. The results can be seen in Figure 28.

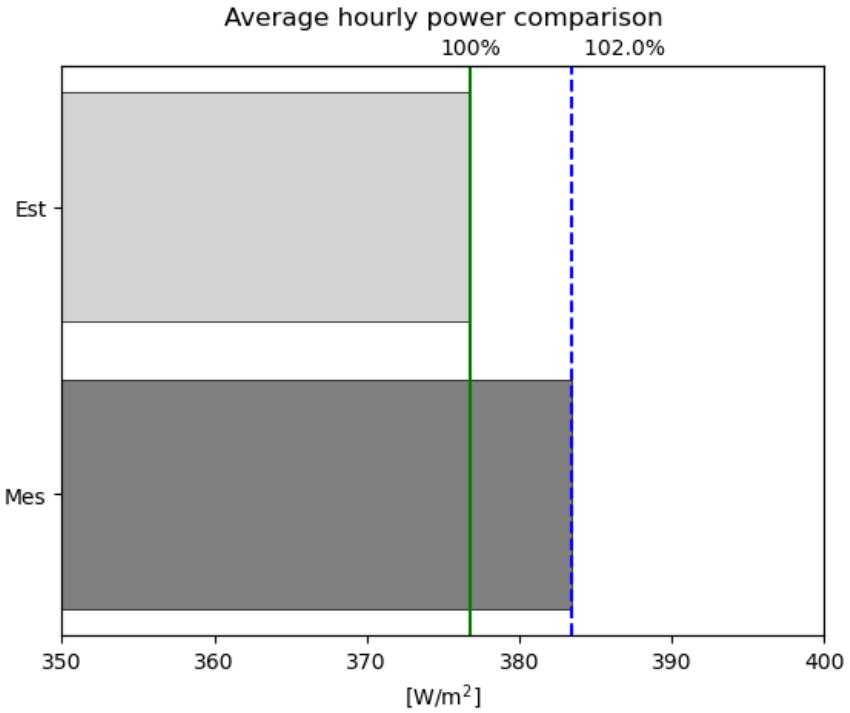

Figure 28: The performance in measure and estimated power for a day where the conditions were met for almost the whole day modeled with estimated "real case": $f_O = 98$, $f_p = 95$ and $f_U = 92.5 => f_{safe} = 86$.

As expected, the average hourly power production difference between the estimated and measured performance is higher, which can be seen in Figure 28. However, this is only due to the estimated power production being lower.

Lastly, the results of estimated and measured power production for a single day using estimated real-world parameters can be seen in Figure 29.

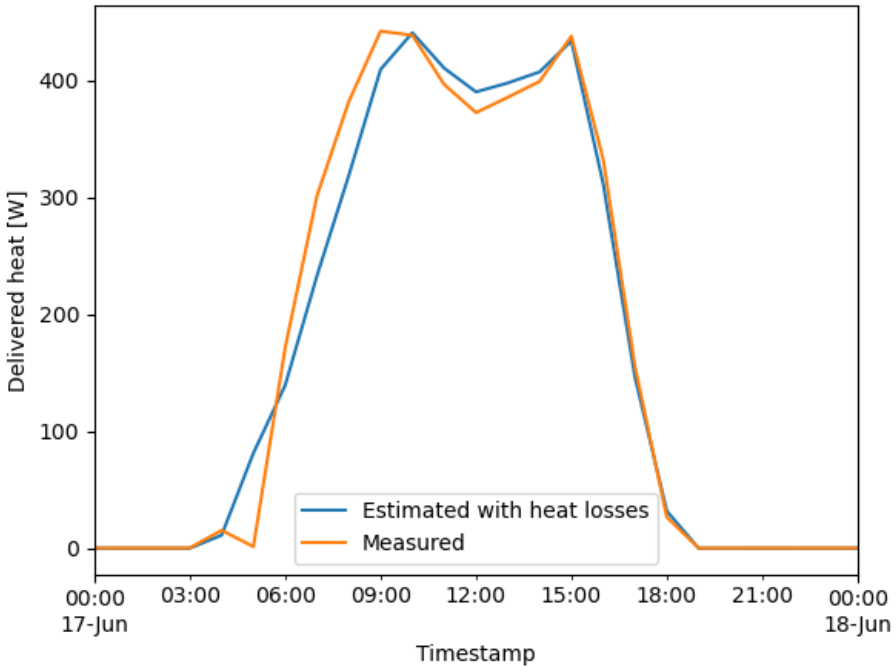

Figure 29: The performance in measured and estimated power for a day where the conditions were met for almost the whole day modeled with estimated "real case": $f_O = 98$, $f_p = 95$and $f_U = 92.5 => f_{safe} = 86$.

Relative to the previous daily power production in Figure 25, the time before 9:00 is even more exaggerated, however, the dip in between 9:00 - 15:00 and is a little bit closer, the time after 15:00 is quite similar where estimated and measured performance is almost the same.

4.2.7 Applying suggested improvements

These results present the increased performance of the solar thermal field if Absolicon would make the suggested fixes in insulation of pipes, and investigating and fixing the tracking system. The insulation of pipes would increase the performance of the park with 3%, see Figure 17 for heat losses, and fixing the tracking system could improve the performance a further 2-3%, see Figure 25. In Figure 30 the comparison between the measured and estimated power output can be seen for the improved case with original ISO evaluation used in Section 4.1.3.

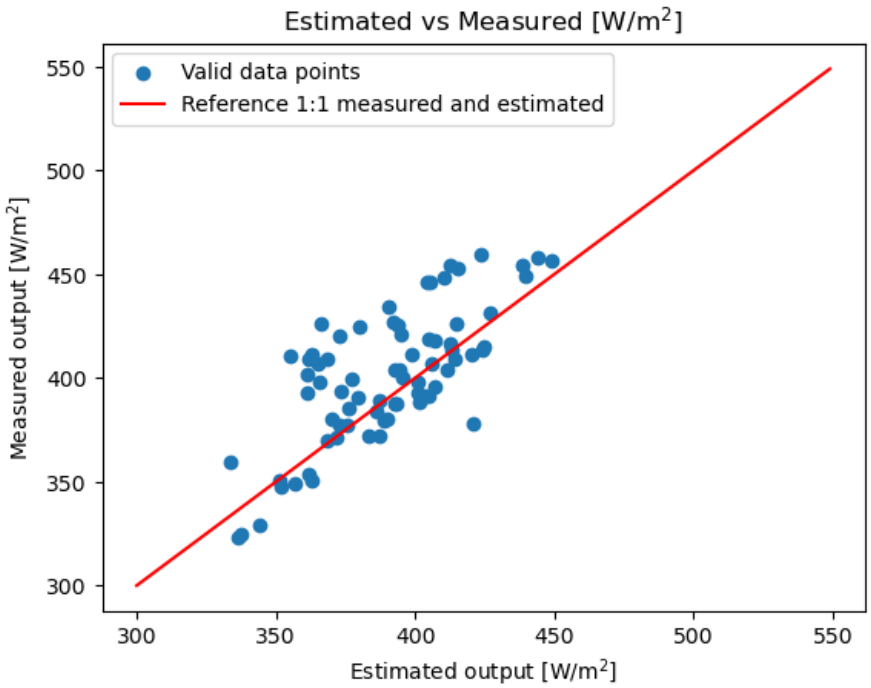

Figure 30: The data points represent the valid measurements for estimated and measured output with $f_{safe} = 0.89$. The linear line represents the 1:1 relationship between estimated and measured power. $f_p = 0.99$, $f_U = 0.9$, and $f_O = 1 => f_{safe} = 0.89$.

It can be seen that there still is a lot of dots below the reference line. This is due to tracking improvement model is just a set percentage and not added directly to the data points. If the performance would be calculated after the suggested improvements would been applied at the park the lower data points would move beyond the reference line and the data points above the reference line would move a little bit down.

A representation of the hourly average measured and estimated power with the same safety factor as before can be seen in Figure 31.

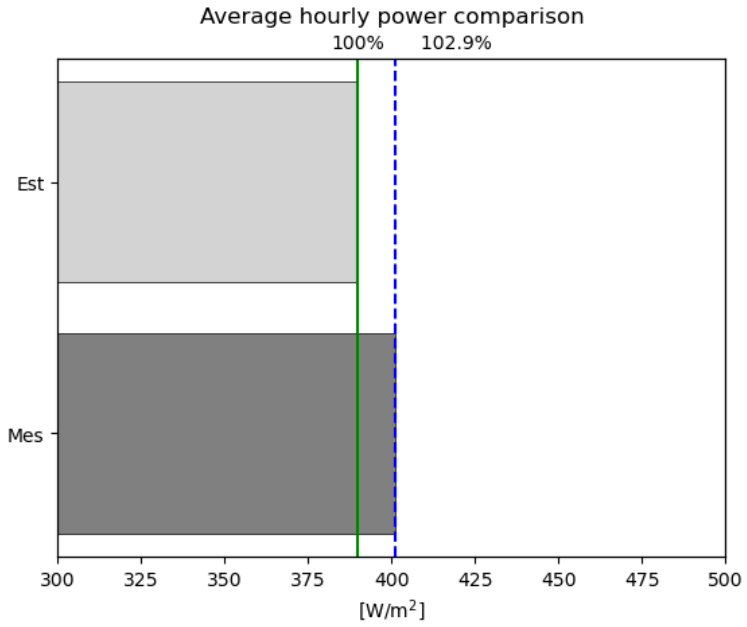

Figure 31: The average hourly power production. The upper bar-plot is the estimated power production with $f_{safe} = 0.89$. The lower bar-plot is the measured power production.

The average hourly measured power consumption is now calculated to 400 W/m^2 which is a increase of 4% relative to the measured power at the actual solar thermal field, see Figure 15. This field would then be verified according to the ISO standard, see Figure 7.

5 Discussion & Conclusion

The evaluation methods that were used were strictly based on the international standardization which gave consistency throughout the report. However, these results only present the peak performance of the solar thermal park. It would therefore be interesting to use a model for performance calculation without simplifications, and then compare and analyze these models. For example, investigate if the gap in the middle of the day would still be present in more accurate power production calculations. And if not rule out that the field is malfunctioning, and investigate why the ISO presents the data wrongly. Using other power production methods would also yield a more accurate result over the year, especially in the autumn and spring. This is due to the irradiance limit in the ISO filtering system, which filters even more data in spring and autumn when the sun is not as strong as in the summer. However, looking at the daily power production it could be seen that in the afternoon the estimated and measured power production was quite similar. But, in the morning and middle of the day the estimated and measured power production was quite different which might be fixed with a more accurate power production method. Using at least one other performance calculation method could more accurately represent the solar field, and could be used to analyze if there could be even more improvements made to the ISO.

Upon reviewing the results for the different performance models an interesting pattern was found, the measured performance is always lower than the estimated performance in the middle of the day. There is no clear explanation for this finding, nonetheless, two explanations are hypothesized: malfunction of the solar thermal park and/or simplified estimations. The malfunctioning of the solar thermal park could be due to non-ideal tracking. This would have the most impact when the beam radiation is the highest, i.e. in the middle of the day. For the case of simplified estimations, it could be both the parameters used in the estimation calculations taken from Solar Keymark or that the estimations from the ISO 241941:2022 do not take into account high beam radiation as well as lower. Considering these hypotheses, the non-ideal solar tracking hypothesis is considered more likely.

Continuing to review the results, there seems to be a fine line between getting verified and not acquiring the verification. As proven, three safety factor parameters alter the estimated performance requirement, f_p, f_U, and f_O, and therefore the verification limit. First, the f_U parameter will be discussed. How accurate the measurement equipment is and how well the equipment is calibrated and maintained could have a big alteration in the uncertainty in measurement factor, f_U, going from 0.95 to 0.9 and inversely. Further on, this could determine whether the solar park gets verified or not. Having a lower accuracy means that it is easier to get verified due to the margin of error in f_{safe} being

larger, this is considered to be one significant fault in this system. This implies that it is harder to get verified with more accurate results by having more expensive/better equipment and keeping them maintained. If the main interest is showing the customer that the field performance is verified by an international performance standard the solar thermal company will most likely buy worse equipment and not maintain it very well. The field would then be more easily verified, show better results and the solar thermal company would save money on investment and maintenance. The conclusion is that this is a loophole that should be fixed. The suggestion for the problem is that f_{safe} could be the same for all equipment, for example, $f_{safe} = 0.95$, but if a solar company uses better equipment and have more maintenance the solar thermal park performance estimation is more reliable. The levels of accuracy could then represent the amount of certainty in the evaluation and not be used as a safety margin. This could potentially be an incentive to get better equipment and show better/more reliable results, beneficial for both the solar thermal company and the client.

It should also be mentioned that the measured performance must be measured with sensors and calculated by using thermodynamics. Therefore, a safety factor of uncertainty in measurements could also be added to the measured performance.

Continuing on the verification process and f_p, the ISO 24194:2022 is simplified by using an empirical equation when calculating heat losses. Looking at the results it is evident that there is a large difference, a factor of three, in heat losses without insulation calculations relative to simplified calculations with the empirically derived formula. However, with calculations for insulated pipes the heat losses in both the magnitude and fluctuation were very similar to the empirically derived heat losses. For better clarification there should be an asterisk mentioning that the empirical derivations are based on insulated pipes or an appendix in the ISO standard with important factors on how the field should be set up for the estimations to be correct. One could also argue that for a field to be correctly installed there should be insulation on the pipes and therefore using the empirical calculations would give approximately the same heat losses as in reality. In conclusion, the solar thermal park should be insulated both to improve the performance and more easily get verified by the ISO. More importantly more emphasis should be put on providing a better performing solar thermal field since Högslätten solar thermal field is a pilot for showcasing the potential of solar thermal in Sweden.

Continuing on the verification process and f_O, this is one factor that would benefit from having a set value. The reasoning behind having a set value is that it is very hard to estimate which other factors than heat losses, collector performance, and measurements could lower the performance of the solar collector field and even when some factors are found they are hard to quantify. For example, the non-ideal flow, to estimate these losses

one has to apply advanced models in flow analysis and probably add more sensors in more places to get a good estimation. Having more advanced models like these would then nullify the simplicity of using the ISO 24194:2022.

Analyzing the irradiance sensitivity, it is evident that the standard performance evaluation does not give the full picture, but rather the peak performance. This could be confusing if the evaluation is used as a tool for predicting and calculating the average performance of the solar thermal field. For example, the actual field performance will be lower due to the heat losses being larger when not in steady-state, this was seen in the f_p sensitivity analysis. If the goal is to get a more complete picture of the solar thermal performance the calculations should be done with more accuracy than empirical equations and over a longer period of time. However, the performance evaluation would probably be quite correct if the performance is compared on a day-to-day basis on sunny days.

Lastly, the solar thermal collector field is not verified according to the requirements stated in the ISO 241941:2022. However, with insulation, tracking system investigation and improvement, and reasonable assumption about other losses the solar thermal field at Högslätten could be verified by all criteria stated in the ISO 24194:2022.

Looking forward and beyond this master's thesis, it would be interesting to see if the evaluation will be the same for different years and for a data set that consists of a whole year. It would also be interesting to see if the calculated estimations of heat losses would correspond to reality if Absolicon makes the suggested improvements of insulating the pipes above ground. It would also be interesting to see if there is a fault in the tracking system, and if there is not, understand why the solar thermal park performance is worse in the middle of the day.

6 References

[1] H. Ritchie, M. Roser, and P. Rosado, "CO_2 and greenhouse gas emissions," *Our World in Data*, 2020. https://ourworldindata.org/co2-and-greenhouse-gas-emissions.

[2] L. Andrén, *Solenergi*. Svensk Byggtjänst, 2011.

[3] REN21, "Renewables 2020 global status report." `https://www.ren21.net/wp-content/uploads/2019/05/gsr_2020_full_report_en.pdf`, 2020. Accessed: 2023-02-16.

[4] IEA, "Solar heat world wide - edition 2022." `https://www.iea-shc.org/Data/Sites/1/publications/Solar-Heat-Worldwide-2022.pdf`. Accessed: 2023-04-02.

[5] IEA, "Heating - fuels & technologies." `https://www.iea.org/fuels-and-technologies/heating`, 2022. Accessed: 2023-01-06.

[6] International Organization for Standardization, "Guide on standardization and quality assurance for solar thermal." `https://solarthermalworld.org/wp-content/uploads/2016/01/estif_standardisation_2012.pdf`. Accessed: 2023-02-14.

[7] International Organization for Standardization, "ISO 24194:2022 - solar energy — collector fields — check of performance." `https://www.iso.org/standard/78074.html`.

[8] E. Magnusson, "Methodology for evaluation of a solar thermal collector field - with an application studying the högslätten thermal collector field," *Umeå University*, 2023.

[9] P. Ollas and Z. Norwood, "Half-time performance assessment of högslätten solar district-heating plant.," 2022. [Unpublished manuscript].

[10] V. Unterberger, V. Kaisermayer, K. Lichtenegger, M. Gölles, and M. Horn, "An adaptive short-term forecasting method for the energy yield of flat-plate solar collector systems," *Applied Energy, Volume 293*, 2021.

[11] Absolicon, "Högslätten-2023-solar-thermal-park." `https://www.absolicon.com/sv/projekt-2/hogslatten-2023-solar-thermal-park/`. Accessed: 2023-03-14.

[12] I. Sarbu and C. Sebarchievici, "Solar heating and cooling systems," *Academic Press*, 2017.

[13] "Solar heat world wide - edition 2022." https://www.absolicon.com/applying-absolicon/solar-collectors-field-twin-group/. Accessed: 2023-04-02.

[14] SolarKeymark, "Database - solar keymark." https://solarkeymark.eu/database/. Accessed: 2023-02-10.

[15] International Organization for Standardization, "Solar thermal collectors — test methods." https://www.iso.org/standard/67978.html. Accessed: 2023-01-09.

[16] S. Venkateshan, *Heat Transfer, Third Edition*. ANE Books Pvt. Ltd, 2021.

[17] S. Frederiksen" and S. Werner, *Fjärrvärme och fjärrkyla*. Studentlitteratur, 2014.

[18] A. Shitzer, "Wind-chill-equivalent temperatures: regarding the impact due to the variability of the environmental convective heat transfer coefficient," 2006.

[19] I. Sarbu and C. Sebarchievici", *Solar Heating and Cooling Systems*. Academic Press, 2017.

[20] J. A. Duffie" and W. A. Beckman, *Solar Engineering of Thermal Processes, Fourth Edition*. Wiley, 2013.

A Appendix - Models

A.1 Python code

The functions that are written are represented in this Appendix together with some important initialization. Due to there being a lot of similar code only the functions and one initialization of a similar function is shown.

A.1.1 Initialize, import and filter data

In the main method the classes where function and plots where made was imported. The dataframe was also initialized.

```
#INIT
from funcs import *
from figuretool import *

df = importDf1h()
df = Q(df)
dfNonFiltered = df
df = filter_ISO24194New(df)
```

Imported all the data of Högslätten and sorted it to the days when all the equipment was working and converted to 1h mean intervals.

```
def importDf1h():
    path = 'CSV-files/Högslätten_data' # Path to where data (.csv files) are stored
    df = import_files(path)
    df = pd.concat(
    [
        df['2022-06-17':'2022-08-11'],
        df['2022-08-15':'2022-08-21'],
        df['2022-08-26':'2022-09-12']
    ])
    #df.index = pd.to_datetime(df.index).tz_localize('Europe/Stockholm')
    #Ta bort localize för skuggning

    df = df.resample('1h').mean()
    return df
```

To import any other data the following code was used.

```python
def importDataNewType(path):
    df = pd.read_csv(path, index_col=[0])
    df.index = pd.to_datetime(df.index)

    dfConcat = pd.concat(
    [
        df['2022-06-17':'2022-08-11'],
        df['2022-08-15':'2022-08-21'],
        df['2022-08-26':'2022-09-12']
    ])
    dfConcat = dfConcat.resample('1h').mean()
    return dfConcat
```

Based on the requirements off the ISO the data was filtered.

```python
def filter_ISO24194New(df):
    df['Hour'] = df.index.hour
    df['Day'] = df.index.dayofyear
    df['windSpeed'] = importDataNewType('CSV-files/Högslätten_data/wind_speed.csv')

    lat = 62.633
    df = skuggning(lat ,df)
    return df[(df['H_shaded'] < 0) & (df['deltaT'] <= 5) & (df['Tam'] >= 5)
    & (df['windSpeed'] <= 10) & (df['Gb'] >= 600) & (df['alpha_s']>= 0)]
```

A.1.2 Measure shadows

To measure shadows the solar angles first had to be calculated.

```python
def solarAzimuthAngle(latitude, df):
    import math
    sind = lambda degrees: np.sin(np.radians(degrees))
    cosd = lambda degrees: np.cos(np.radians(degrees))

    df['theta_z'] = 90 - df['alpha_s']
    nominator = (cosd(df['theta_z'])*sind(latitude) - sind(df['delta']))
    denominator = (sind(df['theta_z'])*cosd(latitude))
    df['gamma_s'] = np.sign(df['w'])*abs(np.rad2deg(np.arccos(nominator/denominator)))
    df['gamma_s'].fillna(0, inplace = True)
    return df
```

```
def solarAltitudeAngle(latitude, df):
    import math
    sind = lambda degrees: np.sin(np.radians(degrees))

    localSolarTime = df['Hour']
    w =  15*(localSolarTime - 12) #hour angle
    df['w'] = w
    df['delta'] = 23.45*np.sin(np.radians(360 * (284 + df['Day'])/365))
    df['alpha_s'] = np.rad2deg(np.arcsin(np.cos(np.radians(latitude))*
    np.cos(np.radians(df['delta']))*np.cos(np.radians(df['w'])) + (np.sin(np.radians(latitude))
    *np.sin(np.radians(df['delta']))))) #Solar altitude angle
    df['solarHeight'] = sind(df['alpha_s'])

    return df
```

The shadows could then be calculated

```
def skuggning(latitude, df):
    sind = lambda degrees: np.sin(np.radians(degrees))
    cosd = lambda degrees: np.cos(np.radians(degrees))
    tand = lambda degrees: np.tan(np.radians(degrees))

    width = 1.095
    S = 1.434 #center to center
    gamma = -90 #Azimuth angle börjar i east

    df = solarAltitudeAngle(latitude, df) #solar altitude angle
    df = solarAzimuthAngle(latitude, df)

    df['beta_ideal'] = np.rad2deg(np.arctan(cosd(df['gamma_s'] - gamma) / tand(df['alpha_s'])))

    nominator = abs(cosd(df['gamma_s'] - gamma)) * abs(sind(df['gamma_s'] - gamma))
    denominator = tand(df['alpha_s'])
    P_y = width*(cosd(df['beta_ideal']) + nominator/denominator)
    df['P_y'] = P_y
    df['H_shaded'] = (1- (S/P_y))*width
    return df
```

A.1.3 Heat losses in pipes

The resistance was calculated with pipe dimensions, the heat losses could then be calculated.

Calculations for heat losses in all pipes with ISO estimations.

```
def calculateHeatLossesISO(r_o, L_pipe, n_pipes, df):
    import math

    T_pipe = (df['SVS_MEAN_GT3']+df['SVS_MEAN_GT1'])/2
    T_a = df['Tam']

    for i in range(len(L_pipe)):
        V_pipe = math.pi*r_o[i]**2*L_pipe[i]*1000
        q1_pipe = 0.32*(V_pipe/L_pipe[i])**(0.22)
        df['PipesISO']  += n_pipes*q1_pipe*L_pipe[i]*(T_pipe - T_a)

    return df
```

Calculations for heat losses in ground pipes.

```
def calculateHeatLossesGroundPipesNew(m_underGround, d_between, k_i, d_i, d_o, L_pipe, df):
    import math
    k_g = 0.3 #Conductivity ground
    T_pipe = (df['SVS_MEAN_GT2']+df['SVS_MEAN_GT1'])/2
    T_a =  df['Tam']
    T_cold = df['SVS_MEAN_GT3']

    for i in range(len(L_pipe)):
        R_c = (d_i[i]/(2*k_g))*math.log(((2*m_underGround/d_between)**2 +1)**0.5)
        R_i = (d_i[i]/(2*k_i))*math.log(d_o[i]/d_i[i])
        R_g = (d_i[i]/(2*k_g))*math.log(4*m_underGround/d_o[i])
        dT = T_pipe - T_a
        df['heat_losses_groundPipes'] += L_pipe[i]*math.pi*d_i[i]*((R_g + R_i)*dT - R_c*
        (T_cold - T_a))/((R_g + R_i)**2 - R_c**2)
    return df
```

Calculations for heat losses in non-insulated pipes above ground.

```
def heatLossesNonInsulated(k_p, r_i, r_o, L_pipe, n_pipes, df):
    import math
    T_pipe = (df['SVS_MEAN_GT3']+df['SVS_MEAN_GT1'])/2
    T_a = df['Tam']
    df = hValue(df)
    for i in range(len(L_pipe)):
        R_p = 1/(2*math.pi*k_p)*math.log(r_o[i]/r_i[i])
        R_f = 1/(2*math.pi*r_o[i]*df['hValue'])
        R_overall  = R_p + R_f
        Q_total = (T_pipe - T_a)*n_pipes*L_pipe[i]/R_overall
        df['heat_Losses_NonInsulatedPipes'] += Q_total

    return df
```

Calculations for heat losses in insulated pipes above ground.

```python
def heatLossesInsulated(k_p, r_1, r_2, k_i, isolationThickness, L_pipe, n_pipes, df):
    import math
    T_pipe = (df['SVS_MEAN_GT3']+df['SVS_MEAN_GT1'])/2
    T_a = df['Tam']
    df = hValue(df)

    for i in range(len(L_pipe)):
        r_3 = r_2[i] + isolationThickness
        R_p = 1/(2*math.pi*k_p)*math.log(r_2[i]/r_1[i])
        R_i = 1/(2*math.pi*k_i)*math.log(r_3/(r_2[i]))
        R_f = 1/(2*math.pi*r_3*df['hValue'])
        R_tot = (R_p + R_i + R_f)
        Q_total = (T_pipe - T_a)*n_pipes*L_pipe[i]/R_tot
        df['heat_Losses_InsulatedPipes'] += Q_total

    return df
```

A.1.4 Performance, estimated and measured

To calculate estimated and measured performance.

```python
def Q(df, m ='sqm', Agf=1160):
    """Input: dataframe df
   output: dataframe with mean temperature of collector array,
   measured and modelled power and all calculated parameters
   """
    #A = 1058 # m², aperture area
    #Agf = 1160 # Field gross area

    # Calculate average temperature of collector array at every time step and add to dataframe
    Tm = np.array(df[['SVS_MEAN_GT2','SVS_MEAN_GT3']].mean(axis=1))

    Qmeasured, cf, rho = measured_output_sqm(df, Tm, Agf)
    Qestimate, F0tot, F0, F1, F2, F5, Kb, deltaT, deltaTdt, Ihemtot, Ghemtot, Gbtot, Gb, Gd = QDT_sqm(df, Tm)

    if m == 'total':
        Qmeasured = Qmeasured * Agf
        Qestimate = Qestimate * Agf

    q_frame = pd.DataFrame({"F0tot":F0tot, "F0":F0, "F1":F1, "F2":F2, "F5":F5,
    "Kb":Kb, "deltaT":deltaT, "deltaTdt":deltaTdt, "Ihemtot":Ihemtot,
     "Ghemtot":Ghemtot, "Gbtot":Gbtot, "Gb":Gb, "Gd":Gd, "Tm":Tm, "cf":cf, "rho":rho,
     "Qestimate":Qestimate, "Qmeasured":Qmeasured}, index=df.index)

    return df.join(q_frame)
```

To get steady state in heat.

```python
def dTdt(df, T):
    """Input: dataframe with all necessary data and evenly spaced timesteps without missing data
    output: dT and dT/dt for timestep i to i - 1 as an array of length of dataframe"""
    # Identify timestep based on first two timestamps (indexes)
    dt = (df.index[2] - df.index[1])

    # Conversion factor to convert timestep to seconds
    dt = np.timedelta64(dt,'s').astype(int)

    deltaT = np.zeros(len(df))

    # deltaT[0] remains 0 (undefined what i-1 is in this case), therefore start calculating at 1
    for i in range(1,len(df)-1):
        deltaT[i] = T[i]-T[i-1]
        # diff[i-1] = dT/dt

    deltaTdt = deltaT/dt
    # plt.plot(df.index,dTdt)
    return deltaT, deltaTdt
```

A.1.5 Plotting the results

The calculated heat losses.

```
##ISO
from funcs import *

n_groups = 16
r_o_pipe26 = 0.0269/2
r_o_pipe60 = 0.0603/2
r_o_metalHoseDN32 = 0.0428/2

df['PipesISO'] = 0

#A-00370
L_pipe = 0.210, 1, 0.204
r_o = r_o_pipe26, r_o_metalHoseDN32, r_o_pipe60
n_pipes = 1
df = calculateHeatLossesISO(r_o, L_pipe, n_pipes, df)

#A-00378
L_pipe= 0.2085*2 + 1.580, 0.655
r_o = r_o_pipe26, r_o_metalHoseDN32
n_pipes = 1/2
df = calculateHeatLossesISO(r_o, L_pipe, n_pipes, df)

#C-pipe
L_pipe= 1.434, 0.221*2
r_o = r_o_pipe26, r_o_pipe26
n_pipes = 3
df = calculateHeatLossesISO(r_o, L_pipe, n_pipes, df)

#Inbetween
L_pipe= 0.122/2, 0.122/2
r_o = r_o_pipe26, r_o_pipe26
n_pipes = 8
df = calculateHeatLossesISO(r_o, L_pipe, n_pipes, df)

df['PipesISO'] = df['PipesISO']*n_groups
df_losses = pd.DataFrame(df['PipesISO'])
```

Estimate power vs measured power plot.

```
x = range(300, 550)
f_u = 0.9
f_heat = 0.99
f_o = 1
f_safe = f_heat*f_u*f_o
dfx = df['Qestimate']*f_safe
dfy = df['QmeasuredImproved']
plt.scatter(dfx, dfy)
plt.plot(x, x, color='red')

plt.xlabel('Estimated output [W/m$^2$]')
plt.ylabel('Measured output [W/m$^2$]')

plt.title('Estimated vs Measured [W/m$^2$]')
plt.legend(['Valid data points', 'Reference 1:1 measured and estimated'])

plt.show()
```

Estimate power vs measured power plot with green lines representing f_{safe} and red line heat losses.

```
dfx = df['Qestimate']
dfy = df['Qmeasured']

plt.scatter(dfx, dfy)

x = np.array(list(range(0, 1000)))

f_u = 0.90
f_o = 0.98
f_heat = 0.97

plt.plot(x, x*f_heat, color='red')
plt.plot(x, x*f_heat + x*(1-f_u*f_o), color='green')
plt.plot(x, x*f_heat - x*(1-f_u*f_o), color='green')
plt.xlabel('Estimated output [W/m$^2$]')
plt.ylabel('Measured output [W/m$^2$]')

plt.xlim(250, 600)
plt.ylim(250, 600)

plt.title('Estimated vs Measured [W/m$^2$]')
plt.legend(['Valid data points', 'With heat losses = 3%', 'Uncertainty in measurments = +-12%'])
plt.show()
```

Estimate power vs measured power plot color coded.

```
x = range(0, 1000)
f_u = 0.925
f_heat = 0.95
f_o = 0.98
f_safe = f_heat*f_u*f_o
dfx = df['Qestimate']*f_safe
dfy = df['Qmeasured']


# Define colormap
cmap = plt.cm.get_cmap('hot')
norm = plt.Normalize(vmin=9, vmax=19)

# Create scatter plot with colors representing hour of the day
plt.scatter(dfx, dfy, c=dfx.index.hour, cmap=cmap, norm=norm)
plt.colorbar()

plt.plot(x, x, color='red')
plt.xlim(300, 500)
plt.ylim(300, 500)

plt.xlabel('Estimated output [W/m$^2$]')
plt.ylabel('Measured output [W/m$^2$]')

plt.title('Estimated vs Measured [W/m$^2$]')
plt.legend(['Valid data points', 'Reference 1:1 measured and estimated'])
```

Average hourly measured and estimated power comparison.

```
f_u = 0.9
f_heat = 0.99
f_o = 1
f_safe = f_heat*f_u*f_o
dfEst = df['Qestimate'].mean()*f_safe
dfMes = df['QmeasuredImproved'].mean()

labels = ['Mes', 'Est']
values = [dfMes, dfEst]
colors = ['gray', 'lightGray']

fig, ax = plt.subplots()
ax.barh(labels, values, color = colors, linewidth=0.5, edgecolor='black')

# Set axis labels and title
ax.set_xlabel('[W/m$^2$]')
ax.set_title('Average hourly power comparison')
ax.set_xlim(300, 500)

# Create second axis for percentages
ax2 = ax.twiny()

# Set position and tick labels for second axis
#ax2.set_position(('axes', 1.1, 0, 0.1))
xlim = ax.get_xlim()
ax2.set_xticks([100/(xlim[1]-xlim[0])*(dfEst-xlim[0]), 100/(xlim[1]-xlim[0])*(dfMes-xlim[0])])
ax2.set_xticklabels(['100%', f"{'                    '}{round(dfMes/dfEst*100, 1)}{'%'}"])
ax2.set_xlim(0,100)
print(round(dfMes/dfEst*100,0))

# Hide spines and set ticks for second axis
ax2.spines['top'].set_visible(True)
ax2.tick_params(axis='x', which='both', length=0)

ax2.axvline(x= (100/(xlim[1]-xlim[0])*(dfEst-xlim[0])), color='g', linestyle='-')
ax2.axvline(x=(100/(xlim[1]-xlim[0])*(dfMes-xlim[0])), color='b', linestyle='--')

plt.show()
```

Daily calculated performance.

```
f_u = 0.90
f_heat = 0.97
f_o = 1
f_safe = f_u*f_heat*f_o
dfNonFiltered['estimateNew'] = dfNonFiltered['Qestimate']*f_safe
dfNonFiltered['estimateNew'].iloc[0:25].plot(legend="Insulated")
dfNonFiltered['Qmeasured'].iloc[0:25].plot(legend="Insulated")
plt.xlabel('Time [hours]')
plt.ylabel('Delivered heat [W]')

plt.legend(['Estimated new','Measured'])

plt.show()
```

B Appendix - Equipment

B.1 Equipment

The thermal sensors that were used are Pt 100s and one Pt 1000. They are located at the following spots:

Description name	Measure temperature	Placement
Pt 100	Heat exchanger, hot side	Technical house
Pt 100	Heat exchanger, hot side	Technical house
Pt 100	Heat exchanger, cold side	Technical house
Pt 100	Heat exchanger, cold side	Technical house
Pt 100	Outflow collector group	Collector group 0-1
Pt 100	Outflow collector group	Collector group 2-3
Pt 100	Outflow collector group	Collector group 4-5
Pt 100	Outflow collector group	Collector group 6-7
Pt 100	Outflow collector group	Collector group 8-9
Pt 100	Outflow collector group	Collector group 10-11
Pt 100	Outflow collector group	Collector group 12-13
Pt 100	Outflow collector group	Collector group 14-15
Pt 1000	Ambient air	Outside technical house

C Appendix - Extensive theory

C.1 Solar thermal technology

As mentioned before there are different kinds of technology for different kinds of scenarios. Focus will be on parabolic through collectors due to they are the type used in the evaluated project. Even though flat plate and evacuated solar collectors are not used in Högslätten a quick summery is still mentioned to understand the different application and reach of solar thermal.

C.1.1 Parabolic through collectors

A fundamental parameter for concentrating solar collector is the concentration ratio, C_r, which is the relationship between the aperture area of the collector, A_a, and the absorber area, A_{abs} [19].

$$C_r = \frac{A_a}{A_{abs}} \tag{16}$$

A larger concentration ratio generally means that the fluid can get to higher temperatures, for parabolic troughs a typically concentration ratio is around 10-30.

C.2 Solar fundamentals

To understand why the energy production from the solar collectors varies over the year it is important to grasp the basic ideas of solar angles and radiation to make correct predictions of the location of the sun and earth. In these sections the basic concepts of solar time, radiation and angles will be looked at and described.

C.2.1 Solar time

Solar time is the apparent time due to the current position of the sun. To convert Coordinated Universal Time (UTC) to solar time, two corrections is needed, the first correction is due the difference between the location of interest meridian (longitude lines), L_{st}, and the meridian for that positions local time, L_{loc}. The second correction is due to the earth's rotation which alters the time when the sun crosses the meridian. To calculate the difference in minutes between solar time and UTC the following equation can be used:

$$Solar\,time - Standard\,time = 4(L_{st} - L_{loc}) + E \tag{17}$$

where E is the equation of time and is expressed as

$$E = 0.017 + 0.43cos(B) - 7.35 * sin(B) - 3.35cos(2B) - 9.36sin(2B) \tag{18}$$

where B is given by

$$B = (n-1)\frac{360}{365} \tag{19}$$

n is the amount of days that has passed in that year since the beginning of the year.

C.2.2 Solar angles

Solar angles describe the relationship between a plane on the surface of earth (of any rotation) relative to the incoming solar radiation and position of the sun. Where the plane is located on earth can be described by longitude and latitude:

Longitude, θ_{long}, is the angular coordinate which goes around the globe, starting from 0 in London and has a negative angle going to the west and positive to the east, $-180° \leq \theta_{long} \leq 180°$.

Latitude, ϕ, is the angular coordinate which serves as north and south position of the earth relative to the equator, where north is positive and south is negative, $-90° \leq \phi \leq 90°$.

The earth rotates around its own axis while rotating around the sun. This is explained and calculated with an hour angle, ω and declination, δ.

Hour angle, ω, is the angular displacement east and west due to the rotation of the earth during the day which rotates 15° per hour around its axis where ω goes from negative in the morning to positive in the afternoon, $-180° \leq \omega \leq 180°$.

Declination, δ, is the angular position of the sun relative to the earths equator when the sun is at the local meridian. North is positive and south is negative, due to the tilt of the earth of 23.45° the declination is between $-23.45° \leq \delta \leq 23.45°$. 0° means that the sun is directly above the equator. δ is approximated by

$$\delta = 23.45sin(360\frac{284+n}{365}) \tag{20}$$

When declination and location is known, solar angles can be used to relate that specific position to the suns position and radiation. Figure 32 illustrates how various angles relate

the collectors surface to the sun.

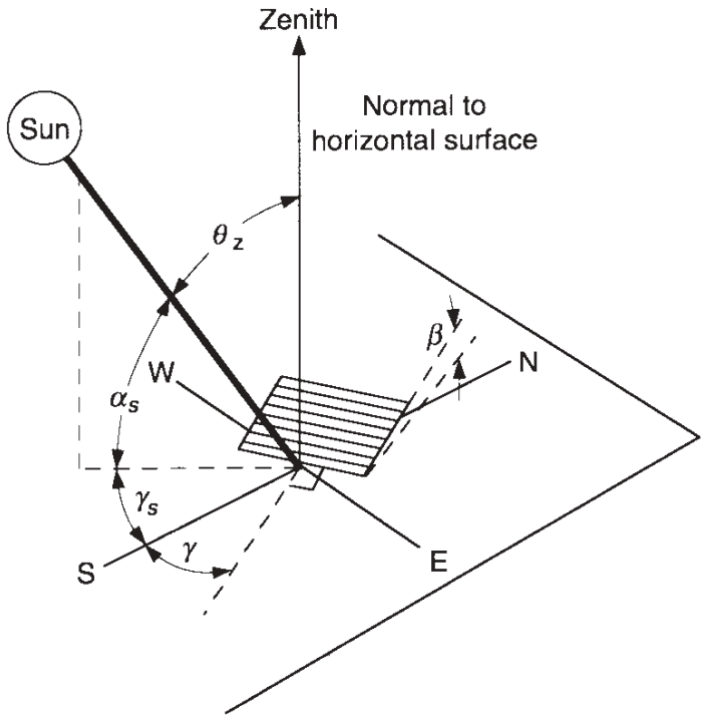

Figure 32: Solar angles for a collector relative to the sun in 3D-space [20]

Solar azimuth angle, γ_s, is the angle between the suns beam radiation normal to the horizontal plane and the south direction, where west is positive and east is negative, $-180° \leq \gamma_s \leq 180°$.

Surface azimuth angle, γ, is the angle between the collectors direction and the south direction, where west is positive and east is negative, $-180° \leq \gamma \leq 180°$.

Tracking angle, β, is the angle between the collector and the horizontal plane.

Zenith angle, θ_z, is the angle between the normal of the horizontal surface and the angle of beam radiation.

Solar altitude angle, α_s, is the angle between the horizontal surface and the angle of beam radiation, the compliment of θ_z, $\alpha_s = 90 - \theta_z$.

Solar altitude, h, is the height between the projection on the horizontal surface and the sun with the solar altitude angle, $h = sin(\alpha_s)$.

Angle of incidence, θ, is the angle between the normal of the collector and the angle of

beam radiation. θ, can be minimized by having a ideal β angle. To achieve minimium angle of incidence the tilt angle should be angled relative to the suns position by using the following relationship

$$\frac{d\theta}{d\beta}(\beta = \beta_{ideal}) = 0 => \beta_{ideal} = tan^{-1}\left(\frac{cos(\gamma_s - \gamma)}{tan(h)}\right) \tag{21}$$

where h is the solar altitude, $h = sin(\alpha_s)$.

C.2.3 Radiation

Beam radiation, G_b, is the direct solar radiation to the earths surface that has not been scattered by the atmosphere. Beam radiation is often also refereed as direct radiation.

Diffuse radiation, G_d is the radiation that has been scattered in the atmosphere while reaching earth.

Total solar radiation, G_{tot}, is the sum of both beam and diffuse radiation.

Air mass, m, is the ratio of beam radiation that passes through the mass of atmosphere to the earths surface relative to the mass the beam radiation passes if the sun is at zenith. For θ_z of 90° the air mass is defined as $m = 1$ and for higher angles the air mass will increase and less radiation will reach earths surface.

$$m = \frac{1}{cos(\theta_z)} \tag{22}$$

C.3 Shadows

Shadows on the collectors could occur due to internal shadowing from collectors shadowing each other or external shadows such as trees. If shadows occur solar collectors perform worse due to less direct radiation.

Internal shadows will emerge when the suns altitude is low, then collector rows will start throwing shadows between themselves. To limit any uncertainties in validating the performance of the field the solar altitude, h, should be large enough to avoid internal shadows between the collectors.

The solar altitude can be calculated with the following formula.

$$sin(h) = cos(\phi)cos(\delta)cos(\omega) + sin(\phi)sin(\delta) \tag{23}$$

To maximize the used land area the collector occupy the collectors could be close to each other causing internal shadows between themselves. Reoccurring internal shadows can be represented with the following figure:

$$P_x = w|sin(\beta)| * \frac{|sin(\gamma^{-3})|}{tan(h)} \tag{24}$$

$$P_y = w(cos(\beta) + |cos(\gamma_s - \gamma)| * \frac{|sin(\gamma_s - \gamma)|}{tan(h)}) \tag{25}$$

$$L_{sh} = max\{0; min(L * N_c + D(N_c - 1) - S\frac{P_x}{P_y}; L * N_c + D(N_c - 1))\} \tag{26}$$

C.4 Heat losses

Heat transfer between materials is the transport of thermal energy due to a temperature difference within the system or across a boundary that separates two systems [16]. The different ways of heat transfer is via conduction, convection and radiation. Conduction happens through materials when there is a spacial temperature gradient between materials, where the material properties alters the amount of heat transferred. Convection is due to a moving fluid carrying away the thermal energy. Radiation is possible without any intervening mediums where thermal radiation happens because of the emission of electromagnetic waves between two surfaces of different temperatures. In this section heat transfer between pipes and surrounding materials will be covered.

Fourier law is used to calculate thermal conductivity for a cross-sectional area that is uniform [16]. The law states that the heat transfer of constant thermal conductivity is

$$q_x = -kA\frac{dT}{dX} \tag{27}$$

Where the temperature is assumed to vary in the x-direction and A is the area of the material.

C.4.1 Pipes above ground

Using Fourier's law for cylindrical forms the heat transfer by conduction is given by:

$$Q_r = 2\pi r(-k\frac{dT}{dr}) \tag{28}$$

If dT is kept constant (steady-state) integration is possible and the heat transfer by conduction is calculated with the following equation:

$$Q_r = 2\pi k\frac{T_{pipe} - T_{amb}}{ln(\frac{r_o}{r_i})} \tag{29}$$

the thermal conduction resistance is then given by

$$R_p = \frac{1}{2\pi k}ln(\frac{r_o}{r_i}) \tag{30}$$

At the outer boundery of the pipe there are heat losses due to convection. The heat losses at the boundary of the pipe due to convection calculated by

$$Q_c = 2 * \pi * r_o * h(T_{outerPipe} - T_{amb}) \tag{31}$$

where the resistance convection at the outer boundary r_o due to the moving air then is

$$R_f = \frac{1}{2\pi r_o h} \tag{32}$$

where h is the heat transfer coefficient of air and is dependent on the wind speed.

The total resistance with and without isolation can now be calculated. The total resistance ***without isolation*** is:

$$R_{total} = R_p + R_f = \frac{1}{2\pi k_p}ln(\frac{r_o}{r_i}) + \frac{1}{2\pi r_o h} \tag{33}$$

and the total resistance ***with isolation*** is:

$$R_{total} = R_p + R_i + R_f = \frac{1}{2\pi k_p}ln(\frac{r_2}{r_i}) + \frac{1}{2\pi k_i}ln(\frac{r_o}{r_2}) + \frac{1}{2\pi r_o h} \tag{34}$$

where r_2 is the outer radius of the innerpipe.

It is now possible to calculate the ***total heat losses*** with the following equation.

$$Q_{total} = L_{pipe} \frac{T_{pipe} - T_{amb}}{R_{total}} \tag{35}$$

using the relevant resistance calculated with equation (34), or equation (33).

D Appendix - ISO

D.1 Safety margin, f_{safe}

The following section is taken directly from the ISO 24194:2022

Three levels for accuracy in the checking can be chosen:

— Level I - giving possibility for giving a very accurate estimate (with low safety retention, e.g. f_{safe} = 0,95) - but with requirements for use of expensive measurement equipment.

— Level II/III - allowing for a less accurate estimate (with higher safety retention, e.g. f_{safe} = 0,90) - but possibility to use less expensive measurement equipment.

f_{safe} is chosen considering potential influences from pipe heat loss, measurement uncertainties, model uncertainties etc. and shall be specified with an accuracy of 2 digits.

f_{safe} is divided into factors considering specific influences. As an example, f_{safe} could be calculated from $f_{safe} = f_P \cdot f_U \cdot f_O$, where:

f_P: Safety factor considering heat losses from pipes etc. in the collector loop. To be estimated based on an evaluation of the pipe losses (e.g. by Formula (23))

f_U: Safety factor considering measurement uncertainty. To be estimated - with the requirements given in 7.2, a factor of 0,95 (level I) and 0,9 (level II and III) can be used – or detailed documentation for the uncertainty calculation is required according to ISO/IEC Guide 98-3.

f_O: Safety factor for other uncertainties e.g. related to non-ideal conditions such as:

— non-ideal flow distribution. To be estimated - should be close to one.

— unforeseen heat losses. To be estimated - should be close to one.

— uncertainties in the model/procedure itself. To be estimated - should be close to one.

f_{safe} Combined safety factor:

$f_{safe} = f_P \cdot f_U \cdot f_O$